CORONAVIRUS

SARS-CoV-2 inflammation durably imprints memory CD4 T cells

Sophie L. Gray-Gaillard[1], Sabrina M. Solis[1], Han M. Chen[1], Clarice Monteiro[1], Grace Ciabattoni[2], Marie I. Samanovic[1], Amber R. Cornelius[1], Tijaana Williams[1], Emilie Geesey[1], Miguel Rodriguez[1], Mila Brum Ortigoza[1], Ellie N. Ivanova[3], Sergei B. Koralov[3], Mark J. Mulligan[1,2], Ramin Sedaghat Herati[1,2]*

Memory CD4 T cells are critical to human immunity, yet it is unclear whether viral inflammation during memory formation has long-term consequences. Here, we compared transcriptional and epigenetic landscapes of Spike (S)–specific memory CD4 T cells in 24 individuals whose first exposure to S was via SARS-CoV-2 infection or mRNA vaccination. Nearly 2 years after memory formation, S-specific CD4 T cells established by infection remained enriched for transcripts related to cytotoxicity and for interferon-stimulated genes, likely because of a chromatin accessibility landscape altered by inflammation. Moreover, S-specific CD4 T cells primed by infection had reduced proliferative capacity in vitro relative to vaccine-primed cells. Furthermore, the transcriptional state of S-specific memory CD4 T cells was minimally altered by booster immunization and/or breakthrough infection. Thus, infection-associated inflammation durably imprints CD4 T cell memory, which affects the function of these cells and may have consequences for long-term immunity.

INTRODUCTION

T cell memory is crucial for durable protection against viral infection and is a well-established correlate of immune protection (*1*–*5*). CD4 T cells make a multifaceted contribution by coordinating innate immune responses, providing help to B cells and CD8 T cells, and directly killing infected cells (*6*, *7*). The quality of memory CD4 T cell responses is typically assessed by interrogation of cellular frequency, cytokine production, provision of help, and T cell receptor (TCR) affinity for antigen (*8*–*11*). Although the goal of vaccination is to induce long-lasting protection, the contribution of inflammation during memory CD4 T cell formation is not well understood.

During the COVID-19 pandemic, some individuals developed CD4 T cell memory to severe acute respiratory syndrome coronavirus 2 (SARS-CoV-2) Spike (S) protein via infection and others via SARS-CoV-2 vaccination. SARS-CoV-2 infection and mRNA vaccination induce durable and robust S-specific CD4 T cell responses skewed toward a type 1 T helper (T_H1) and T follicular helper profile (*12*–*17*). Moreover, infection- and vaccination-derived S-specific CD4 T cells rapidly expand after exposure to S protein during subsequent SARS-CoV-2 vaccination or infection, demonstrating effective recall of memory CD4 T cells (*18*–*20*). Thus, mRNA vaccination and SARS-CoV-2 infection each induce comparable frequencies of memory CD4 T cell responses.

Aside from quantitative induction of a memory CD4 T cell response by vaccine or virus, little is known about whether, or even if, infection- and vaccine-derived memory CD4 T cells qualitatively differ given differences in the inflammatory context in which S epitopes are presented. Factors during initial priming such as inflammatory signals, site and persistence of antigen exposure, cell-to-cell interactions, and cytokine milieu imprint resulting memory pools and influence T cell responses upon antigen re-exposure (*21*, *22*). Viral infection triggers high levels of inflammation in contrast with that present during immunization (*23*). Serum levels of inflammatory cytokines in patients with COVID-19 positively correlate with disease severity when compared with healthy controls (*24*–*26*). By contrast, serum levels of inflammatory cytokines are low after vaccination (*27*), and only mild reactogenicity has been reported (*28*–*30*). The presence of concomitant inflammation may have consequences for T cell memory. Reduced TCR diversity, decreased frequency of antigen-specific memory T cells, and impaired cytokine production have been reported in the setting of excess inflammation (*31*–*33*). The impact of infection-associated inflammation on S-specific memory CD4 T cells remains unexplored. A better appreciation of how inflammation affects memory T cell quality can therefore improve our understanding of SARS-CoV-2 infection–derived protective immunity and inform future vaccine design strategies.

Because of the difference in inflammatory context between infection and vaccination at the time of memory CD4 T cell priming, we hypothesized that qualitative differences in S-specific memory CD4 T cells may have been established. To test this hypothesis, we explored the transcriptional and epigenetic profiles of S-specific CD4 T cell responses in individuals whose first exposure to S protein was either infection (infection-primed) or immunization (vaccine-primed). These data highlight the importance of understanding how the inflammatory environment during initial antigen exposure shapes memory CD4 T cell development.

RESULTS

S-specific CD4 T cells form a distinct cluster in the AIM assay

We sought to understand the extent to which concomitant inflammation affected the generation of S-specific memory CD4 T cells and subsequent responses after re-exposure to S antigens, given the transcriptional differences observed between the acute response to vaccination and infection (*23*, *26*, *27*). Beginning in 2020, we longitudinally followed individuals after diagnosis of acute COVID-19 or

[1]Department of Medicine, New York University Grossman School of Medicine, New York, NY, USA. [2]Department of Microbiology, New York University School of Medicine, New York, NY, USA. [3]Department of Pathology, New York University School of Medicine, New York, NY, USA.
*Corresponding author. Email: ramin.herati@nyulangone.org

after initiation of mRNA vaccination, as previously described (*12*, *34*). From this cohort, we randomly selected 22 individuals with samples available from approximately 8 months after their second vaccination—hereafter referred to as the pre-booster time point—and 1 month post-booster to longitudinally assess immune memory (Fig. 1A and fig. S1A). Eleven of these individuals had not been previously infected with SARS-CoV-2, as confirmed by N-protein enzyme-linked immunosorbent assay at the time of initial mRNA vaccination, and their first exposure to S protein was therefore via mRNA vaccination (labeled "vaccine-primed"). The other 11 individuals had confirmed diagnoses of SARS-CoV-2 infection in the spring of 2020 (labeled "infection-primed") and received two doses of mRNA vaccination approximately 9 months later. They then received their third vaccination approximately 20 months after the onset of COVID-19 (tables S1 to S3). Among these 11 infection-primed participants, 10 had mild or minimally symptomatic COVID-19, and 1 had severe disease (table S2). Participants' ages ranged from 28 to 62, with a median age of 42.5 for infection-primed individuals and 39 for vaccine-primed individuals (table S1).

To identify vaccine- and infection-primed participants' S-specific memory CD4 T cells, we used the activation-induced marker (AIM) assay (*12*, *35*–*42*). After overnight stimulation with overlapping S peptides, S-specific CD4 T cells were identified on the basis of the coexpression of activation markers such as CD69, CD137, and CD200 (Fig. 1B and fig. S1B). Stimulated cells demonstrated higher frequencies of $CD69^{+}CD137^{+}$ CD4 T cells than paired unstimulated controls (fig. S1C). Both cohorts demonstrated an increase in S-specific CD4 T cells after booster (Fig. 1C and fig. S1D) and had similar frequencies at both time points (fig. S1E), suggesting that a third dose of mRNA vaccination elicited a CD4 T cell response, as reported previously (*43*, *44*).

We next probed epitope-specific CD4 T cell responses using an HLA-DPB1*04:01 allele tetramer loaded with peptides 167 to 180 of S protein (TFEYVSQPFLMDLE, $S_{167–180}$) (*39*). We interrogated circulating $S_{167–180}$-specific $CD45RA^{-}$ CD4 T cells 1 month after booster vaccination and observed similar frequencies between cohorts (Fig. 1D and fig. S1F). Moreover, the frequency of $S_{167–180}$-specific $CD45RA^{-}$ CD4 T cells correlated with AIM-responding CD4 T cells (Fig. 1E and fig. S1G). The frequency of S-specific CD4 T cells measured by the AIM assay was higher than that of $S_{167–180}$-specific CD4 T cells, which is plausible given that the AIM assay assesses specificity for epitopes covering the entirety of S protein whereas tetramer assesses specificity for a single peptide.

However, we observed subtle differences between vaccine- and infection-primed S-specific memory CD4 T cells, such as for protein expression of CD45RA and CCR7 (Fig. 1F). To more deeply profile the differences between the S-specific memory CD4 T cells in vaccine- and infection-primed participants, we evaluated the transcriptional state of S-specific CD4 T cells using droplet-based multimodal single-cell RNA sequencing (scRNA-seq) [expanded cellular indexing of transcriptomes and epitopes by sequencing (exCITE-seq)] (*45*) for 14 randomly selected participants after AIM assay (fig. S1A) and subsequent magnetic bead enrichment for CD69 and CD137, two surface proteins highly expressed by S-specific cells (Fig. 1B and fig. S1I) (*12*, *38*). Single cells from 33 samples were integrated for downstream analyses after quality control (fig. S1H). In total, we recovered 127,047 CD4 T cells. Dimension reduction was performed on gene expression to generate a uniform manifold approximation and projection (UMAP). Using graph-based clustering (*46*), we identified four major clusters (Fig. 1G and fig. S1J), including one cluster of 11,919 cells labeled as "S-specific CD4 T," which enriched for genes associated with T cell activation (*37*) such as *TNFRSF4* (OX40), *TNFRSF9* (CD137), *TFRC* (CD71), and *LTA* (Fig. 1H and fig. S1K). Gene ontology analysis of genes differentially expressed by S-specific CD4 T cluster compared with the nonnaïve CD4 T cluster demonstrated enrichment for terms such as "cellular response to stimuli" and "TCR signaling" (Fig. 1I). Thus, an AIM-activated subset of CD4 T cells was readily identified by scRNA-seq.

To further assess antigen specificity of the S-specific CD4 T cell cluster, we evaluated TCR sequences. The S-specific cluster TCRs were generally not observed in any other cluster and were highly clonal (Fig. 1J). We then compared the S-specific CD4 TCRβ sequences with an independently generated database of approximately 3000 class II TCRβ sequences (*47*). For 8 of 14 participants, there was substantial overlap between the S-specific CD4 T cell CDR3 amino acid sequences and those of the public SARS-CoV-2 TCRβ database (Fig. 1K) (*47*), although TCR overlap was not observed in all participants, perhaps because of the relatively limited number of TCRβ sequences available for comparison. The majority of TCRs in the S-specific cluster mapped to peptides 160 to 218 of S protein (Fig. 1L), which was reported to contain immunodominant CD4 T cell epitopes (*39*, *40*). Thus, multimodal single-cell profiling after AIM permits the transcriptional and clonotypic evaluation of S-specific memory CD4 T cells.

Infection-primed S-specific CD4 T cells exhibit a cytotoxic profile

Prior studies described expression of T_H1 cytokines, including interferon-γ (IFN-γ), tumor necrosis factor, and interleukin-2 (IL-2), after SARS-CoV-2 infection and vaccination (*12*–*14*, *17*, *18*, *39*, *48*, *49*). Moreover, cytotoxic S-specific memory CD4 T cells produce granzyme B after SARS-CoV-2 infection (*50*–*52*). Overnight stimulation with S peptides induced more *GZMB*, *IFNG*, *IL2*, and *TNF* transcripts in the S-specific CD4 T cluster relative to non-activated CD4 T cells (Fig. 2A and fig. S2A). To investigate whether vaccine- and infection-primed S-specific memory CD4 T cells demonstrated different functionality, we compared the expression of these transcripts. *IL2* expression was higher for vaccine-primed participants, whereas *GZMB* expression was higher in the infection-primed cohort, at both the pre- and post-booster time points (Fig. 2B). Because polyfunctional CD4 T cell responses are a correlate of protection (*10*), we assessed differences in polyfunctionality in S-specific CD4 T cells from vaccine- and infection-primed cohorts at both time points. S-specific CD4 T cell polyfunctionality was largely similar across cohorts, with little change in these transcripts due to booster immunization (Fig. 2C and fig. S2B). Thus, both types of memory priming result in robust T_H1 effector responses, concordant with previous studies (*17*, *18*, *38*).

To evaluate the distribution of the S-specific CD4 T cells subset more broadly, we applied dimensionality reduction with 27 parameters to the S-specific CD4 T cluster, which revealed 11 unique clusters (Fig. 2, D and E). The distribution of cells across these 11 clusters was similar between pre- and post-booster time points for both cohorts (fig. S2C). Cluster 0, which was enriched for *TCF7*, *CD27*, and *SELL*, contained the majority of S-specific CD4 T cells and was similar between cohorts. However, S-specific CD4 T cells from infection-primed participants had more cells in cluster 1, which enriched for *GZMB*, than from vaccine-primed participants after

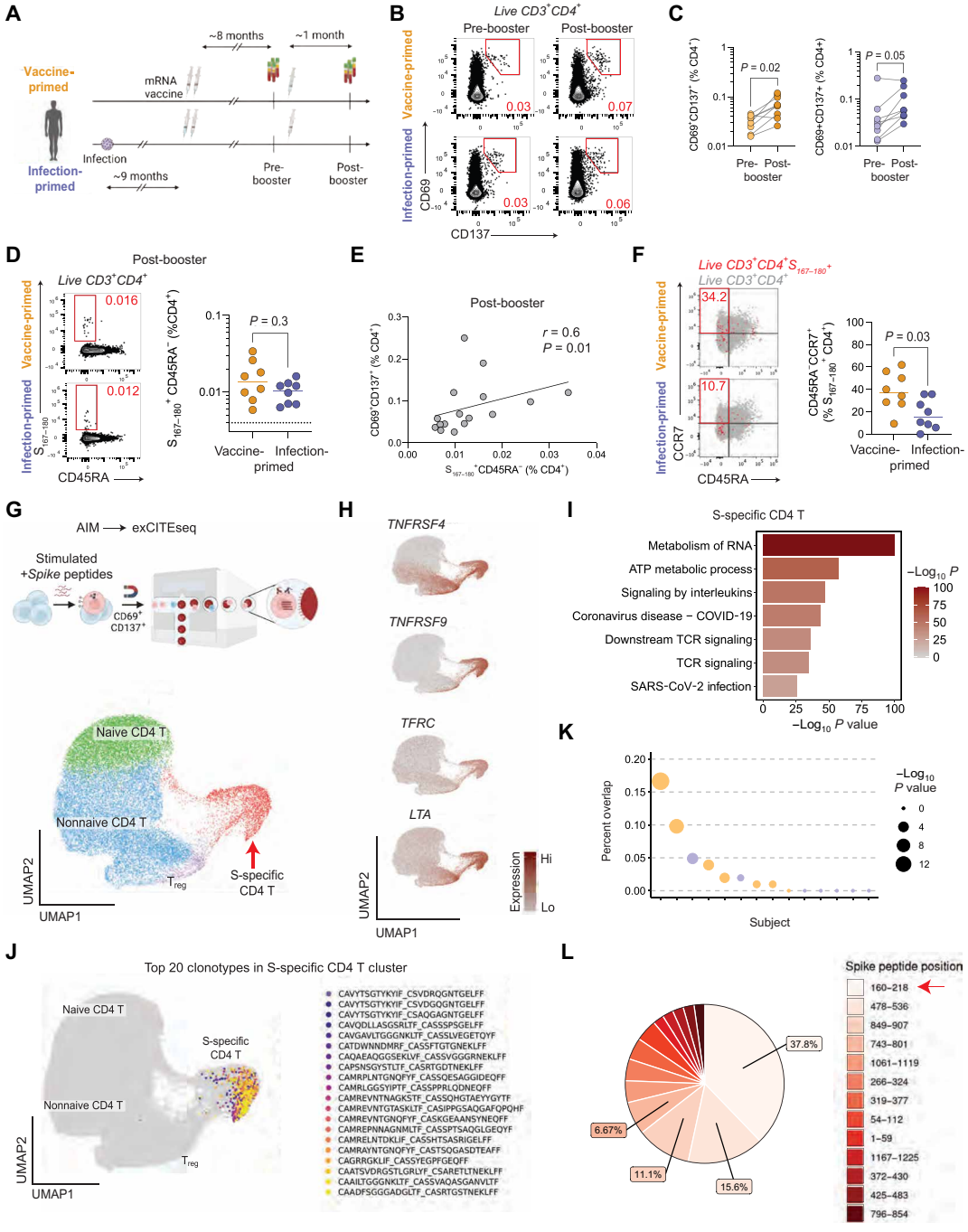

Fig. 1. S-specific CD4 T cells form a distinct cluster in the AIM assay. (**A**) Cohort design of COVID-19 vaccine–primed and SARS-CoV-2 infection–primed adults receiving third dose of BNT162b2 vaccine. Pre-booster and post-booster sampling events are indicated. (**B**) Representative flow cytometry plots for vaccine- and infection-primed participants' CD4 T cells at pre-booster and post-booster time points for expression of CD69 and CD137 after the AIM assay. Frequency shown in red. (**C**) Summary data for PBMC from vaccine-primed (orange, $n = 8$) and infection-primed (purple, $n = 8$) participants after AIM assay. *P* values by Wilcoxon matched-pairs signed-rank test. (**D**) $S_{167–180}$ HLA class II tetramer and CD45RA expression plots for vaccine- and infection-primed participants at the post-booster time point. Summary data shown for vaccine-primed (orange, $n = 8$) and infection-primed (purple, $n = 8$) participants. Statistical significance was determined by Wilcoxon test. Frequency shown in red. (**E**) Spearman correlation between frequency of $CD69^+CD137^+$ CD4 T cells after AIM and the frequency of $S_{167–180}{}^+$ CD4 T cells at the post-booster time point ($n = 16$). (**F**) Representative plots for CD45RA and CCR7 expression by $S_{167–180}{}^+$ CD4 T cells from vaccine- and infection-primed participants. Data from the same experiment in (D). *P* value by Wilcoxon test. Frequency shown in red. (**G**) Experimental design schematic. UMAP projection of CD4 T cells from the AIM assay, pooled across samples and clustered using gene expression. (**H**) Scaled expression of *TNFRSF4* (OX40), *TNFRSF9* (CD137), *TFRC* (CD71), and *LTA*. (**I**) Gene ontology for DEGs at adjusted $P < 0.05$ for S-reactive CD4 T cell compared with CD4 T cell cluster. (**J**) Top 20 clonotypes by frequency in the S-reactive CD4 T cluster. (**K**) Per-participant TCR overlap between S-reactive CD4 TCRs and the Adaptive Biotechnologies SARS-CoV-2–reactive TCR database. (**L**) Distribution of epitope specificity of S-reactive CD4 T cells as inferred from the reference SARS-CoV-2 TCRβ dataset. See also fig. S1. T_{reg}, regulatory T cell; ATP, adenosine triphosphate.

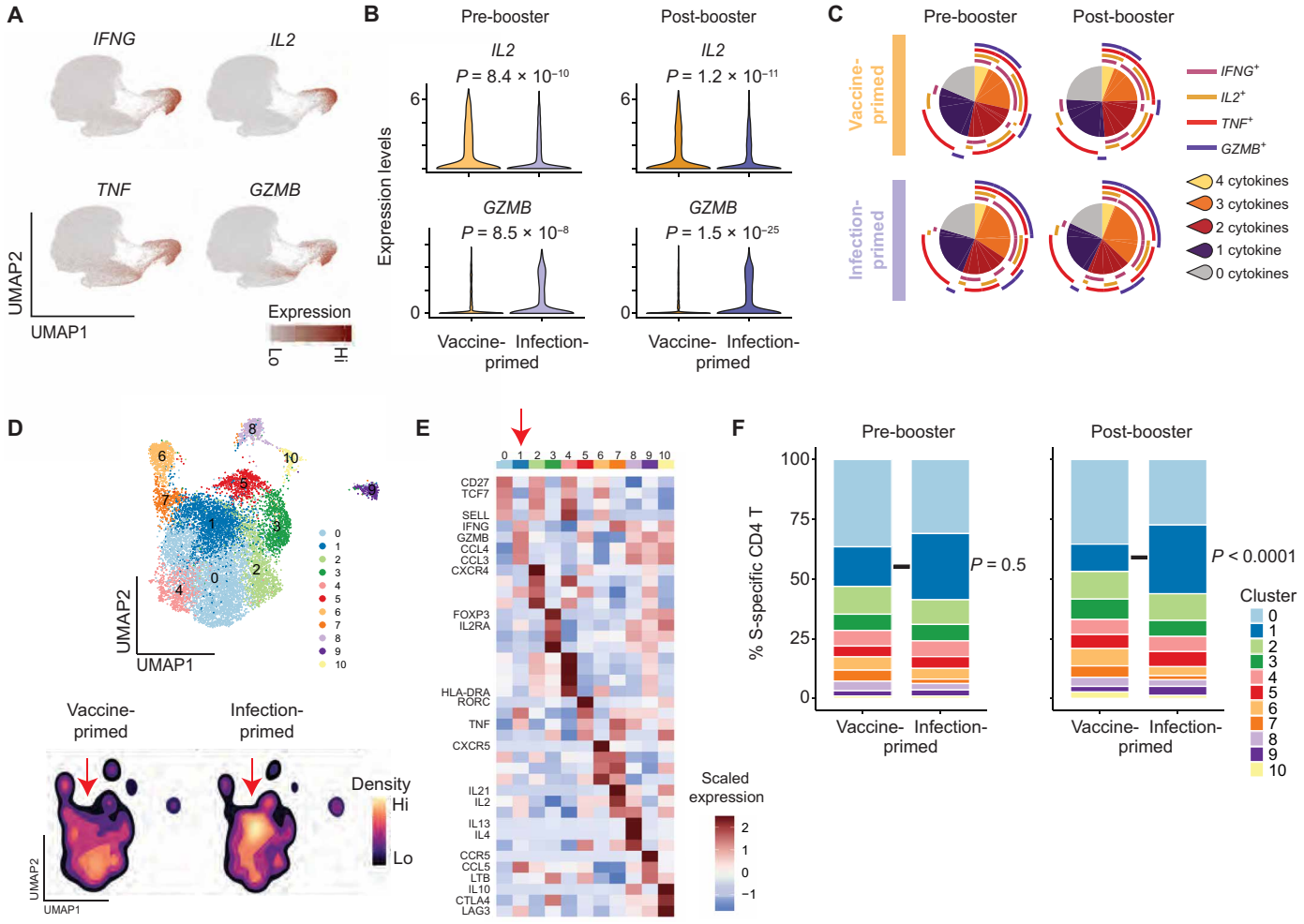

Fig. 2. Infection-primed S-specific CD4 T cells exhibit a cytotoxic profile. (**A**) Scaled expression of *IFNG*, *IL2*, *TNF*, and *GZMB*. (**B**) Scaled expression for *IL2* and *GZMB* between cohorts at pre- and post-booster time points. Nominal *P* values reported. (**C**) Polyfunctionality analysis. (**D**) S-specific CD4 T cells projected onto UMAP and clustered for gene expression of 27 selected parameters. UMAP colored by density and split by cohort. (**E**) Scaled expression of DEGs at adjusted $P < 0.01$ for each cluster. (**F**) Vaccine-primed versus infection-primed S-specific CD4 T cell cluster distribution at pre- and post-booster time points [unpaired two-way analysis of variance (ANOVA) with Šidák's post hoc test]. See also fig. S2.

booster vaccination (Fig. 2, D to F, and fig. S2D). Thus, infection-primed S-specific CD4 T cells contain a greater proportion of cytotoxic cells compared with vaccine-primed S-specific CD4 T cells. Moreover, the functional capability of S-specific CD4 T cells is largely unchanged after repeated mRNA vaccinations, including in infection-primed participants.

Inflammation during priming results in durable transcriptional effects in S-specific CD4 T cells

Given the differences observed between the cohorts using a subset-focused analysis (Fig. 2), we next asked whether the broader transcriptional profile of S-specific CD4 T cells differed by cohort. Principal components analysis (PCA) of the post-booster S-specific CD4 T cells revealed separation of vaccine- and infection-primed participants (Fig. 3A). To identify the genes driving the differences between cohorts, we performed differential gene expression analysis of the S-specific CD4 T cluster before and after booster immunization. Between S-specific memory CD4 T cells from vaccine- and infection-primed participants, there were 317 genes differentially expressed pre-booster and 755 genes differentially expressed post-booster (fig. S3, A and B, and data S1), which were not observed in analysis of other clusters (fig. S3C). *CCR7* expression was enriched in vaccine-primed S-specific CD4 T cells at both time points, which corroborated our previous observation of differential surface protein expression of CCR7 by flow cytometry in $S_{167-180}^{+}$ CD4 T cells (Fig. 1E). However, *CCR7* expression—a proxy for differentiation state of the memory CD4 T cells—did not drive the observed differences between the cohorts (fig. S3D). S-specific CD4 T cells from vaccine-primed individuals differentially expressed genes such as *NFKB2*, *NFKBIA*, *NFKBID*, *NFKBIZ*, and *REL*, which may reflect differential nuclear factor κB (NF-κB) signaling. By contrast, S-specific CD4 T cells from infection-primed individuals differentially expressed genes such as *GZMB*, *HLAB*, *IFI6*, *IFITM1*, and *IFITM3*, which are interferon-stimulated genes (ISGs) (Fig. 3B) (*53*). Thus, vaccine- and infection-primed S-specific CD4 T cells have distinct transcriptional profiles.

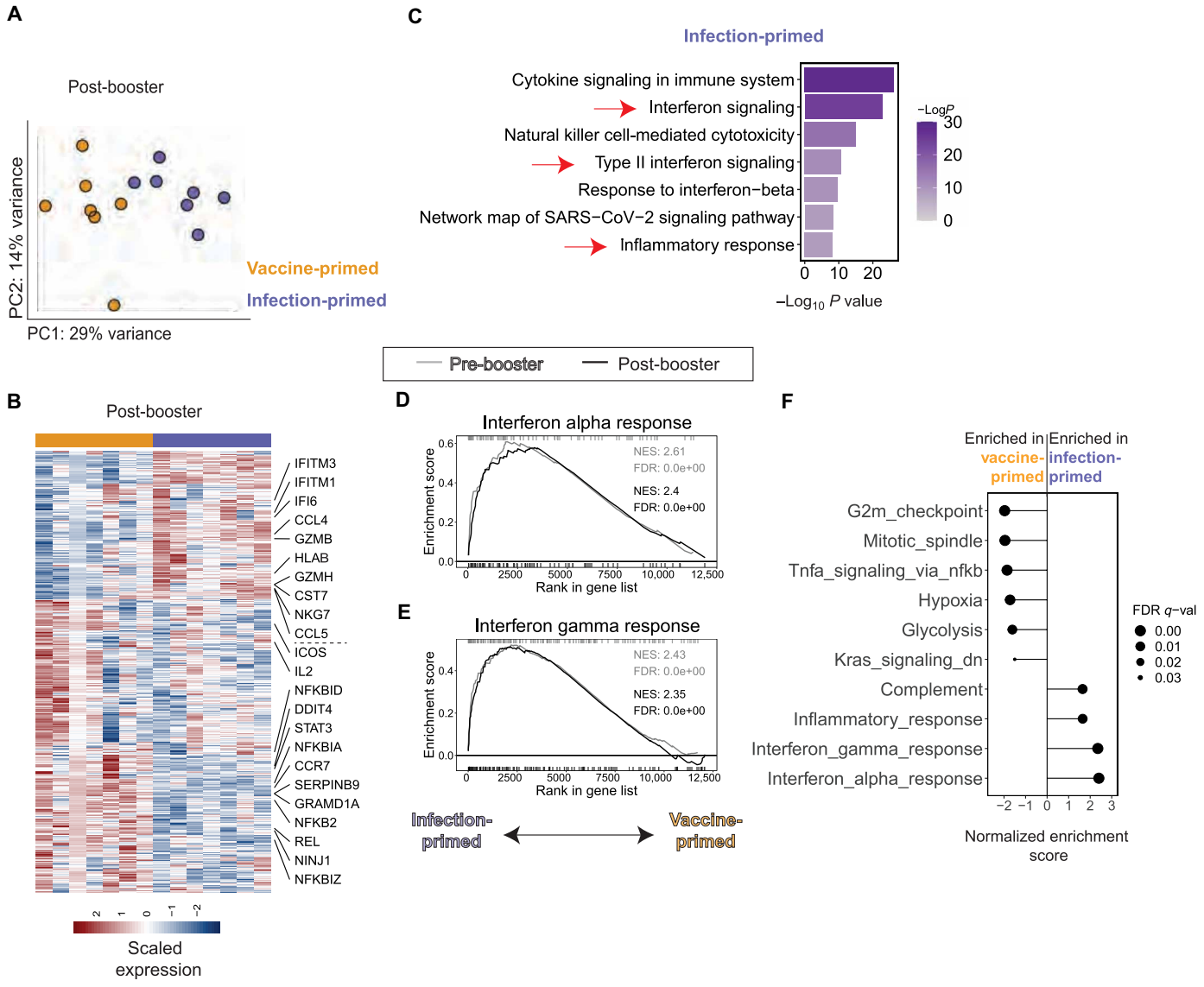

Fig. 3. Inflammation during priming results in durable transcriptional effects in S-specific CD4 T cells. (**A**) PCA of post-booster vaccine-primed (orange) and infection-primed (purple) S-specific CD4 T cells. Each symbol indicates one participant. (**B**) Heatmap of DEGs between post-booster vaccine- and infection-primed cohorts. (**C**) Gene ontology analysis for DEGs at adjusted $P < 0.05$ for infection-primed S-specific CD4 T cells at post-booster time point. (**D** and **E**) GSEA for (D) interferon alpha response and (E) interferon gamma response gene sets for S-specific CD4 T cells. The light gray line indicates the pre-booster time point, and the dark gray line indicates the post-booster time point. NES, normalized enrichment score. (**F**) GSEA results for hallmark gene sets enriched at FDR < 0.05 post-booster. Positive enrichment scores denote enrichment toward the infection-primed cohort in (D) to (F). See also fig. S3.

We next evaluated the coordinated gene expression of the infection-primed S-specific CD4 T cells. Gene ontology analysis of differentially expressed genes (DEGs) (Fig. 3B and fig. S3B) denoted strong enrichment of terms for "interferon signaling" and "inflammatory response" (Fig. 3C). Gene set enrichment analysis (GSEA) (*54*) revealed enrichment for "interferon alpha response" and "interferon gamma response" gene sets in S-specific CD4 T cells from infection-primed individuals at the pre- and post-booster time points (Fig. 3, D and E; fig. S3E; and data S2). Several other gene sets including inflammatory response were differentially enriched in infection-primed individuals (Fig. 3F and fig. S3E). Booster immunization did not substantially change the gene set enrichment (Fig. 3, D and E, and fig. S3E). Thus, S-specific memory CD4 T cells primed during infection and recalled by mRNA vaccination sustain an inflammatory imprint characterized by increased ISG expression compared with cells from vaccine-primed individuals.

Vaccine-primed and infection-primed S-specific CD4 T cells have distinct epigenetic landscapes

Given durability of the inflammatory imprint across time and S re-exposure (Fig. 3), we wanted to evaluate whether the infection- versus vaccine-derived transcriptional signatures were encoded at an epigenetic level (Fig. 4A; fig. S4, A and B; and table S2). We profiled S-specific CD4 T cells using AIM followed by the transcriptomics,

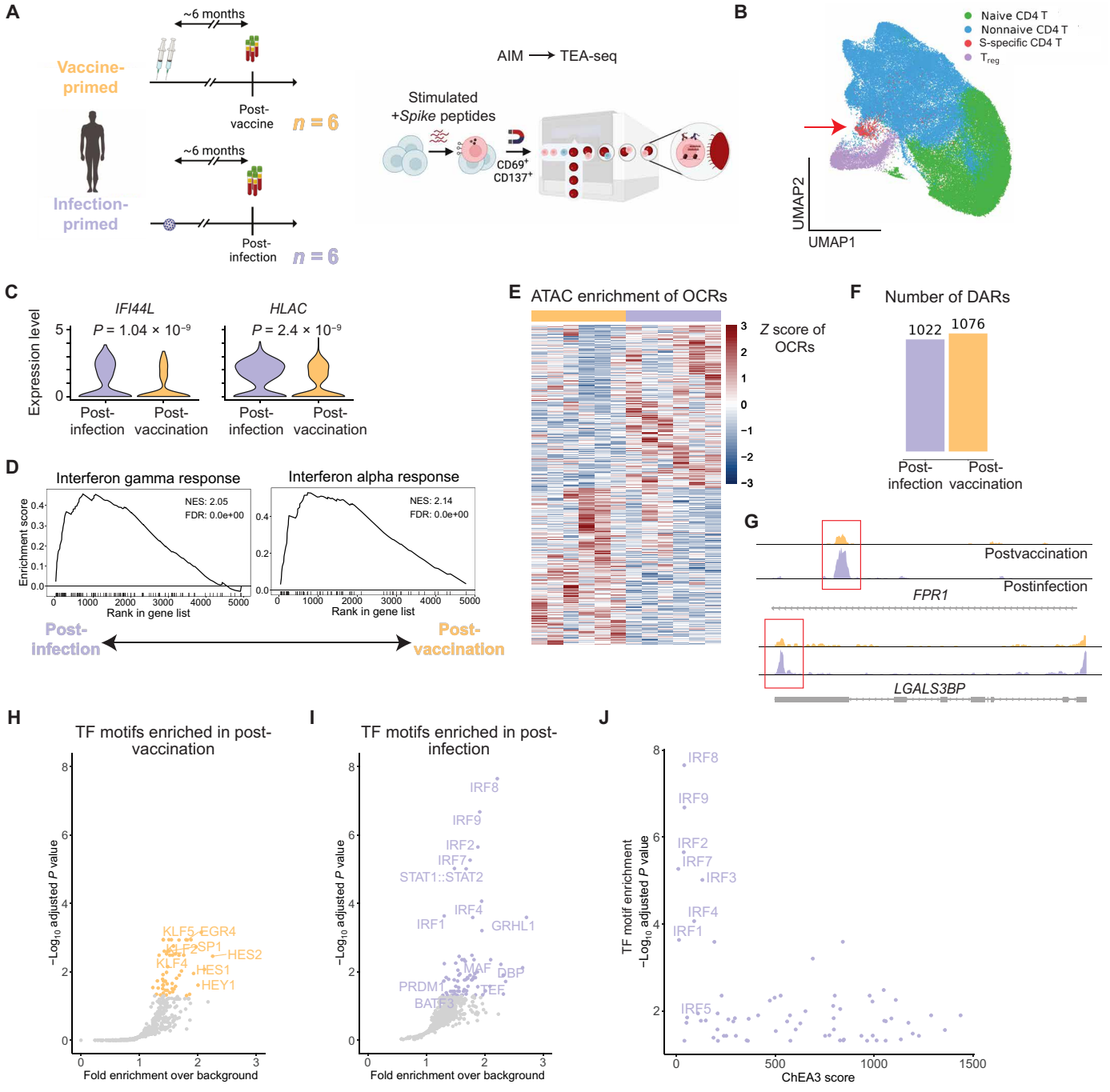

Fig. 4. Vaccine-primed and infection-primed S-specific CD4 T cells have distinct epigenetic landscapes. (**A**) Study schematic of postvaccine and postinfection sampling events for mRNA vaccine-primed and SARS-CoV-2 infection–primed adults, respectively. (**B**) UMAP of stimulated CD4 T cells pooled across samples and clustered for gene expression. (**C**) Difference in scaled expression for *IFI44L* and *HLAC* between postinfection and postvaccination samples. Nominal *P* values shown as determined by DESeq2. (**D**) GSEA for interferon alpha response and interferon gamma response gene sets for transcriptional profiling of S-specific memory CD4 T cells. Positive enrichment scores indicate enrichment for the postinfection cohort. (**E**) Heatmap OCRs in the S-specific CD4 T cells postvaccination (yellow) and postinfection (purple). (**F**) Number of DARs shown (E) at a nominal *P* value of <0.05. (**G**) Representative ATAC-seq tracts shown at the *FRP1* and *LGALS3BP* loci. (**H** and **I**) Enrichment of TF-binding motifs over background in the top differentially accessible OCRs based on nominal *P* value of $<5 \times 10^{-3}$ in (H) postvaccination S-specific memory CD4 T cells and (I) postinfection S-specific memory CD4 T cells. (**J**) TFs shown for the $-\log_{10} P_{adj}$ value from postinfection OCR motif analysis against the TF predicted by ChEA3 using the infection-primed gene expression data. See also fig. S4.

epitopes, and chromatin accessibility assay (TEA-seq) (*55*). Dimensionality reduction and clustering based on gene expression revealed a cluster of S-specific CD4 T cells that differentially expressed transcripts associated with activation (Fig. 4B and fig. S4C). S-specific CD4 T cells postinfection differentially expressed ISGs such as *IFI44L* and *HLAC* and demonstrated strong enrichment for interferon alpha response and interferon gamma response gene sets by GSEA compared with S-specific CD4 T cells from postvaccination individuals (Fig. 4, C and D, and data S3). These transcriptional differences indicate that imprinting during differentiation is already evident 6 months after priming. Genome-wide chromatin mapping revealed that the majority of open chromatin regions (OCRs) were located in intergenic regions and introns (fig. S4D and data S4). The S-specific CD4 T cluster demonstrated increased accessibility of regions near activated gene loci (fig. S4E). We next performed analysis of differentially accessible regions (DARs) between postinfection and postvaccination and identified 2098 DARs (Fig. 4, E and F). Consistent with the transcriptional data, ISG loci had more OCRs in postinfection than in postvaccination S-specific CD4 T cells, such as was observed in the *FPR1* and *LGALS3BP* loci (Fig. 4G). Thus, there is an epigenetic basis for the differential transcriptional profiles in S-specific memory CD4 T cells after infection or vaccination.

To determine which signaling pathways could have been most relevant to the transcriptional profiles observed, we performed transcription factor (TF) motif analysis of OCRs. The postvaccination S-specific CD4 T cells enriched for hairy and enhancer of split-1 (HES) family TFs (Fig. 4H), underscoring the role of Notch signaling for CD4 T cell memory formation (*56*–*59*). By contrast, postinfection S-specific CD4 T cells had motif enrichment for interferon regulatory factor (IRF) family TFs and signal transducers and activators of transcription 1 (STAT1) to STAT2 motifs (Fig. 4I). IRF family TFs are known to directly influence the differentiation of CD4 T cells (*60*–*63*). Moreover, enriched motifs from OCRs were concordant with the ChEA3-predicted TF regulation (*64*) derived from genes up-regulated in infection-primed post-booster (Fig. 4J) and postvaccination samples (fig. S4F). Thus, the inflammatory context surrounding memory CD4 T cell formation appears to result in epigenetic changes that may bias subsequent activation to cognate antigen.

Breakthrough infection minimally alters the transcriptional profile of S-specific CD4 T cells

The inflammation-associated transcriptional imprint in infection-derived S-specific memory CD4 T cells remained largely unchanged despite multiple mRNA vaccinations (Fig. 3). This raised the question of whether vaccine-derived memory CD4 T cells would be reimprinted with the transcriptional changes associated with inflammation after exposure to S protein in the context of breakthrough infection. Breakthrough SARS-CoV-2 infection occurred in 6 of the 11 vaccine-primed participants at a median of 5 months after third vaccination, during a time when the Omicron strain was predominant. The peripheral blood of these individuals was collected 1 month after onset of symptoms (Fig. 5A; fig. S1A; and table S1). All breakthrough infections were mild and did not require hospitalization (table S3), similar to that of SARS-CoV-2 infections in the infection-primed cohort.

Prior studies have described the induction of S-specific memory CD4 T cells in circulation, which peaks around 5 to 7 days after the onset of symptoms and returns to prebreakthrough frequencies by day 30 (*19*, *20*). The circulating frequency of S-specific CD4 T cells 1 month after SARS-CoV-2 breakthrough infection as assessed by AIM was comparable to matched post-booster (prebreakthrough) samples from the same individuals (Fig. 5B). Moreover, frequencies of S-reactive CD4 T cells after breakthrough SARS-CoV-2 infection did not differ from that of infection-primed participants (Fig. 5C).

We next tested whether vaccine-primed S-specific memory CD4 T cells can be transcriptionally imprinted because of concomitant inflammation of breakthrough infection. PCA once again demonstrated separation between vaccine- and infection-primed cells driven by PC2. Moreover, post-breakthrough vaccine-primed responses did not cluster independently of post-booster vaccine-primed samples (Fig. 5D), suggesting transcriptional similarity between the post-booster and post-breakthrough S-specific CD4 T cells from vaccine-primed individuals. Despite breakthrough infection, cluster 1 remained enriched in infection-primed S-specific CD4 T cells relative to post-breakthrough vaccine-primed S-specific CD4 T cells (Fig. 5E). Infection-primed S-specific CD4 T cells differentially expressed *CCL5*, *GZMB*, and *HLAB* compared with post-breakthrough S-specific CD4 T cells, whereas relatively few genes were differentially expressed between post-breakthrough and post-booster vaccine-primed S-specific CD4 T cells (Fig. 5, F and G, and data S5). Thus, breakthrough infection resulted in only subtle differences in differential gene expression in S-specific CD4 T cells relative to prebreakthrough.

Furthermore, pathway-level transcriptional changes by GSEA demonstrated enrichment of interferon alpha response and interferon gamma response gene sets in the infection-primed S-specific CD4 T cells relative to the post-breakthrough vaccine-primed S-specific CD4 T cells (Fig. 5, H and I; fig. S5C; and data S6). Moreover, there was no increased enrichment for the interferon alpha response gene set in S-specific CD4 T cells from post-breakthrough vaccine-primed cells relative to post-booster vaccine-primed cells (Fig. 5J). Thus, breakthrough infections minimally alter the transcriptional profiles of established S-specific memory CD4 T cells, supporting the notion of transcriptional stability in S-specific memory CD4 T cells.

Clonotypes enriched for the vaccine-primed gene signature can undergo inflammatory imprinting by breakthrough infection

We next wanted to examine heterogeneity in the transcriptional profiles at single-cell resolution. To do this, we derived a "vaccine signature" and an "infection signature" from the post-booster DEGs (fig. S3B) and determined each cell's molecular imprint scores by gene set variation analysis (GSVA) (Fig. 6A and fig. S6A) (*65*). The largest proportion of vaccine-primed S-specific CD4 T cells was enriched for the vaccine signature, whereas the largest proportion of infection-primed cells was enriched for the infection signature (Fig. 6, B and C, and fig. S6B). S-specific memory CD4 T cells maintained positive enrichment for the vaccine signature and negative enrichment for the infection signature despite breakthrough infection (Fig. 6D and fig. S6C).

Prior studies have shown heterogeneous outcomes of individual CD4 T cell clones (*11*). To assess transcriptional profiles at a clonotypic level after multiple S exposures, we identified the top four expanded clonotypes observed at all time points for each cohort and performed GSVA analysis for vaccine and infection signatures (Fig. 6E). Infection-primed clonotypes were relatively homogeneous

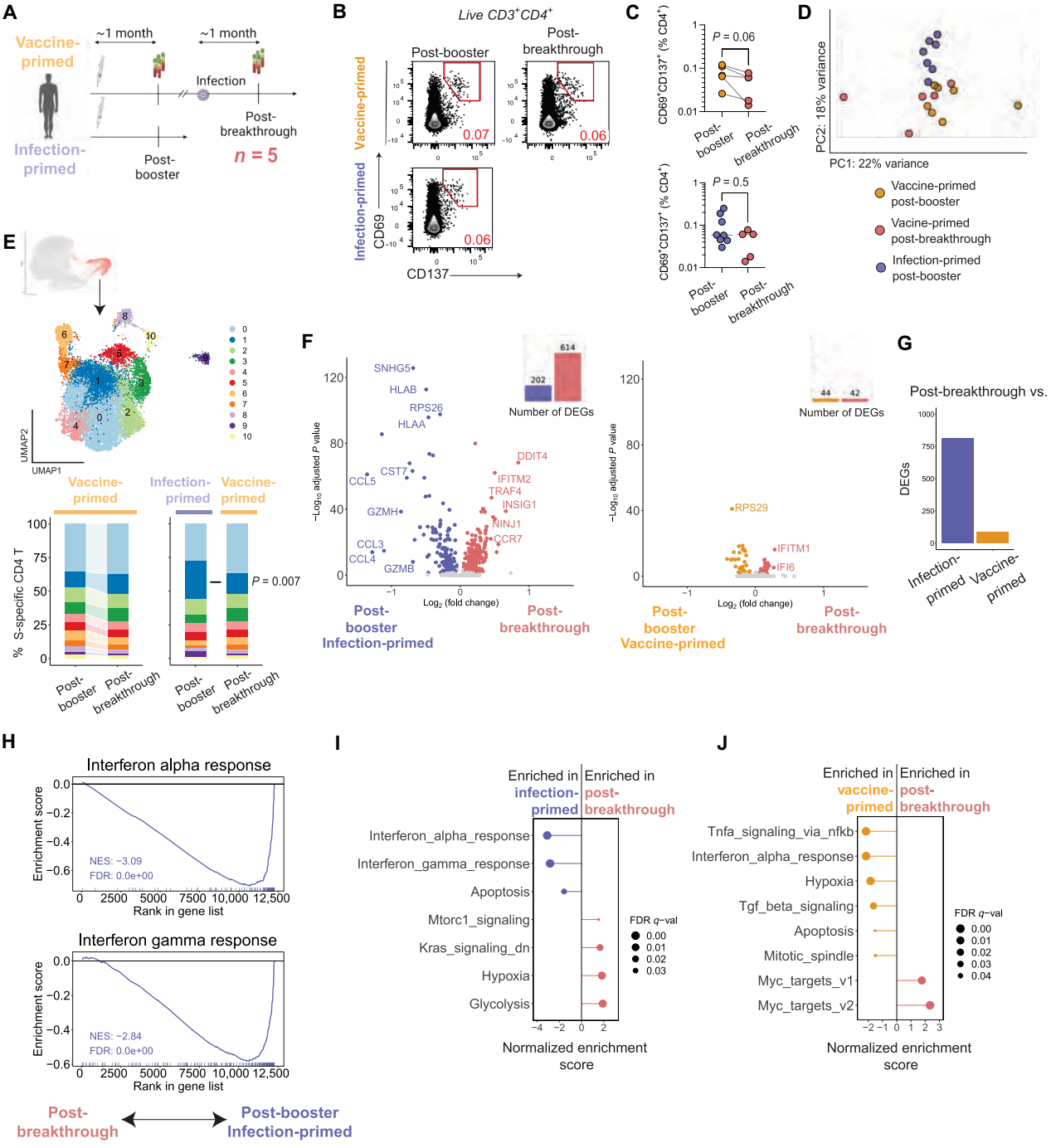

Fig. 5. Breakthrough infection minimally alters the transcriptional profile of S-specific CD4 T cells. (**A**) Breakthrough SARS-CoV-2 infection in vaccine-primed adults after third dose of BNT162b2 vaccine. (**B**) Representative flow plots for post-booster vaccine– and infection-primed participants and post-breakthrough samples for expression of CD69 and CD137 after AIM assay. Frequency shown in red. The example shown is from the same participant as in Fig. 1B. (**C**) Summary plots of $CD69^+CD137^+$ coexpression in CD4 T cells at post-booster and post-breakthrough time points. *P* values by Wilcoxon matched-pairs signed rank test (top) and Wilcoxon unpaired test (bottom). (**D**) PCA of transcriptional profiling of post-booster vaccine-primed (orange) and infection-primed (purple) and post-breakthrough (red) S-specific CD4 T cells. Each symbol indicates one participant. (**E**) S-specific CD4 T cells projected onto UMAP and clustered as described in Fig. 2D. Bar graphs of vaccine- versus infection-primed S-specific CD4 T cell cluster distribution at post-booster and post-breakthrough time points (two-way ANOVA with Šidák's post hoc test). (**F**) Volcano plot showing DEGs at adjusted $P < 0.05$. Genes in purple denote enrichment in infection-primed S-specific CD4 T cells, orange for vaccine-primed post-booster S-specific CD4 T cells, and red for post-breakthrough S-specific CD4 T cells. (**G**) Summary bar graph of DEGs in (F). (**H**) GSEA interferon alpha response and interferon gamma response gene sets in infection-primed samples. (**I** and **J**) GSEA for Hallmark gene sets at FDR < 0.05 when comparing (I) infection-primed, post-booster samples with post-breakthrough and (J) vaccine-primed, post-booster samples with post-breakthrough. Positive enrichment scores denote enrichment for the post-breakthrough samples, and negative enrichment scores signify enrichment for post-booster samples. See also fig. S5.

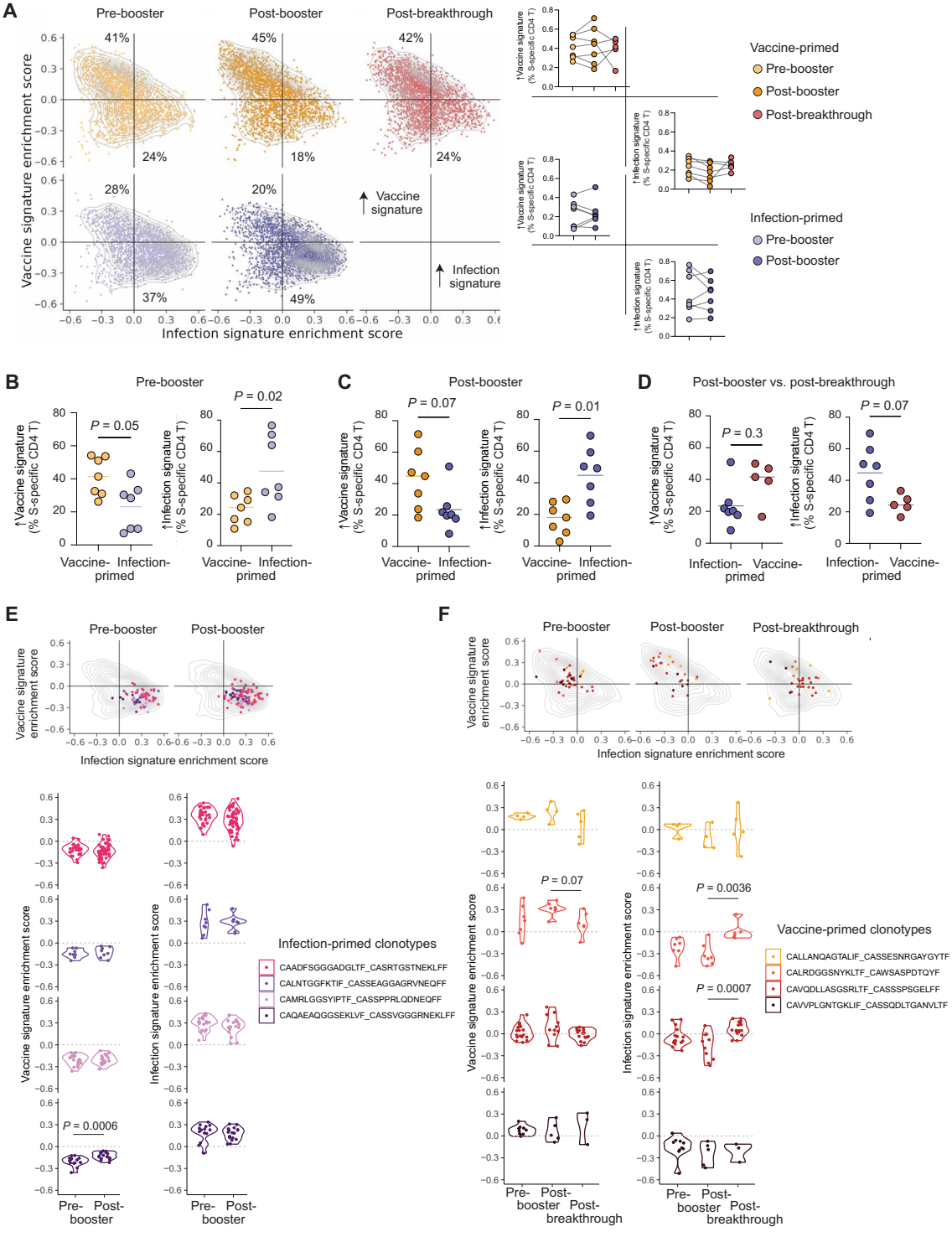

Fig. 6. Clonotypes enriched for the vaccine-primed gene signature can undergo inflammatory imprinting by breakthrough infection. (**A**) GSVA-derived enrichment scores for the "vaccine" and "infection" signatures plotted in two-dimensional Cartesian space for S-specific CD4 T cells pooled from all individuals and split by time point and cohort. Median frequencies of first and third quadrants in black. Summary plots for each individual shown. (**B** to **D**) Summary data at each time point. *P* values by Wilcoxon test. (**E** and **F**) Enrichment scores for the vaccine and infection signatures for (E) the four clonotypes from infection-primed participants and (F) vaccine-primed participants that repeated in all time points shown. *P* values by Wilcoxon test. See also fig. S6**.**

in their scores for both vaccine and infection signatures and demonstrated minimal change due to booster vaccination. Two vaccine-primed clonotypes had increased in infection signature scores after SARS-CoV-2 breakthrough infection (Fig. 6F). Thus, re-exposure to antigen in the context of high levels of inflammation may alter the transcriptional profiles of memory CD4 T cells in a clonotype-specific manner.

Infection-primed transcriptional signature confers a proliferative disadvantage

We next wanted to test whether transcriptional inflammatory imprinting affected functional properties of S-specific memory CD4 T cells. We examined the coordinated gene expression in vaccine-primed S-specific CD4 T cells, as was previously done for infection-primed cells (Fig. 3). Gene ontology analysis of DEGs in vaccine-primed S-specific CD4 T cells revealed terms for "cell cycle" and "NF-κB signaling" (Fig. 7A and fig. S3B), whereas GSEA evinced strong enrichment for "mitotic spindle" and "G_2M checkpoint" signatures (Fig. 7, B and C, and fig. S3C). Thus, vaccine-primed S-specific CD4 T cells express higher levels of genes related to proliferation.

To directly compare proliferative capacity, we tested the in vitro expansion of post-booster peripheral blood mononuclear cells (PBMCs) from vaccine- and infection-primed samples in response to S peptide (Fig. 7D). CD4 T cells from vaccine-primed individuals proliferated more strongly than cells from infection-primed individuals by approximately twofold (Fig. 7E and fig. S7, A and B). We also measured B cell responses and plasmablast differentiation to assess T cell help to B cells in vitro, as peptide stimulation leads to B cell proliferation driven by activated CD4 T cells (*66*). The frequency of $CD71^+CTR^{lo}$ B cells from vaccine-primed individuals was fourfold higher than from infection-primed individuals (Fig. 7F). B cell proliferation correlated with S-specific CD4 T cell proliferation in both cohorts (Fig. 7G). Similarly, frequencies of cultured $CD38^+CD27^+$ plasmablasts were three times higher from vaccine-primed individuals than from infection-primed individuals (Fig. 7H). Moreover, the majority of plasmablasts were CTR^{lo}, indicating that these cells differentiated throughout the course of the 5-day culture (fig. S7C). Plasmablast expansion also correlated with S-specific CD4 T cell expansion in both cohorts (Fig. 7H). Thus, inflammatory imprinting is associated with impaired proliferative capability of S-specific memory CD4 T cells in vitro.

DISCUSSION

Memory CD4 T cell responses make an important contribution to protective immunity, yet the molecular characteristics required for high-quality memory CD4 T cells responses are not well understood. Using the AIM assay, we profiled the transcriptional and epigenetic landscape of S-specific CD4 T cells in participants whose first exposure to S protein was either mRNA vaccination or SARS-CoV-2 infection and arrived at several notable findings. First, we uncovered a durable transcriptional signature of inflammation, which included genes such as *CCL3*, *CCL4*, *CCL5*, and *GZMB* in infection-primed S-specific CD4 T cells relative to vaccine-primed S-specific CD4 T cells. Second, S-specific memory CD4 T cells established by infection had distinct epigenetic landscapes likely shaped by IRF family TFs. Third, breakthrough SARS-CoV-2 infection in vaccine-primed individuals did not grossly alter the transcriptional profile of S-specific memory CD4 T cells, indicating resistance of memory CD4 T cells to further imprinting. Last, vaccine-primed S-specific CD4 T cells were enriched for mitotic spindle and G_2M checkpoint signatures and showed a proliferative advantage in vitro over infection-primed S-specific CD4 T cells. These observations suggest that the quality of inflammation at the time of CD4 T cell priming has lasting effects on CD4 T cell memory.

Adaptive immune responses are the basis for long-term effective protection against pathogens, yet little is understood about why protection is durable in some scenarios and short-lived in others. In this study, inflammation due to viral infection left a transcriptional signature in infection-primed S-specific CD4 T cells. IFN signaling plays a central role in the immune response to COVID-19 (*67*–*70*) and was associated with induction of cytotoxic CD4 T cells in patients with COVID-19 (*52*). Consistent with the concept that IFN signaling is important to T cell differentiation and proliferation (*71*, *72*), IFN alpha receptor (IFNAR) blockade reduces granzyme B expression in virus-specific CD4 T cells (*73*). However, the effects of type I IFN timing and dose on memory CD4 T cell differentiation and maintenance are largely unknown. Further studies of IFN signaling during CD4 T cell memory differentiation will be needed to provide a mechanistic understanding of the consequences of the inflammation-induced transcriptional and functional imprinting observed here.

To assess malleability of the transcriptional imprint, we considered re-exposure to S protein in high and low inflammation settings on the transcriptional profiles of vaccine- and infection-primed S-specific memory CD4 T cells. Longitudinal analysis of S-specific CD4 T cells suggested subtly increased ISG expression after breakthrough infection, including at a clonotypic level, although future studies will be needed to determine whether this represents reimprinting or the detection of newly differentiated memory CD4 T cells. Our data further suggest an epigenetic basis for the transcriptional imprinting, given that S-specific memory CD4 T cells had greater chromatin accessibility near ISG loci, along with enrichment for IRF family TF-binding sites motifs, compared with vaccine-primed S-specific CD4 T cells. How long these epigenetic changes persist is not yet known, but memory CD8 T cells and epigenetic landscapes can remain stable over many years (*74*). Moreover, our analyses indicate that there are measurable effects of inflammatory imprinting on the functional properties of memory CD4 T cells. Vaccine-primed S-specific memory CD4 T cells were enriched for proliferative transcriptional programs, and these cells outperformed infection-primed cells in an in vitro proliferation assay. Additional studies will be needed to determine whether and how altered cellular responses due to inflammatory imprinting affect outcomes during secondary infection.

In conclusion, the imprint of inflammation during S-specific memory CD4 T cell differentiation results in persistent transcriptional, epigenetic, and functional alterations, which are sustained. Similarly, SARS-CoV-2 breakthrough infection does not markedly alter the transcriptional profile of vaccine-primed memory CD4 T cells. The transcriptional stability observed in memory CD4 T cells highlights the relevance of inflammatory signaling during memory differentiation, and the resistance to reimprinting observed here has major implications for rational vaccine design.

MATERIALS AND METHODS

Study design

We examined T cell responses in adults receiving a third dose of BNT162b2 vaccine at the time points indicated (Fig. 1A). After written

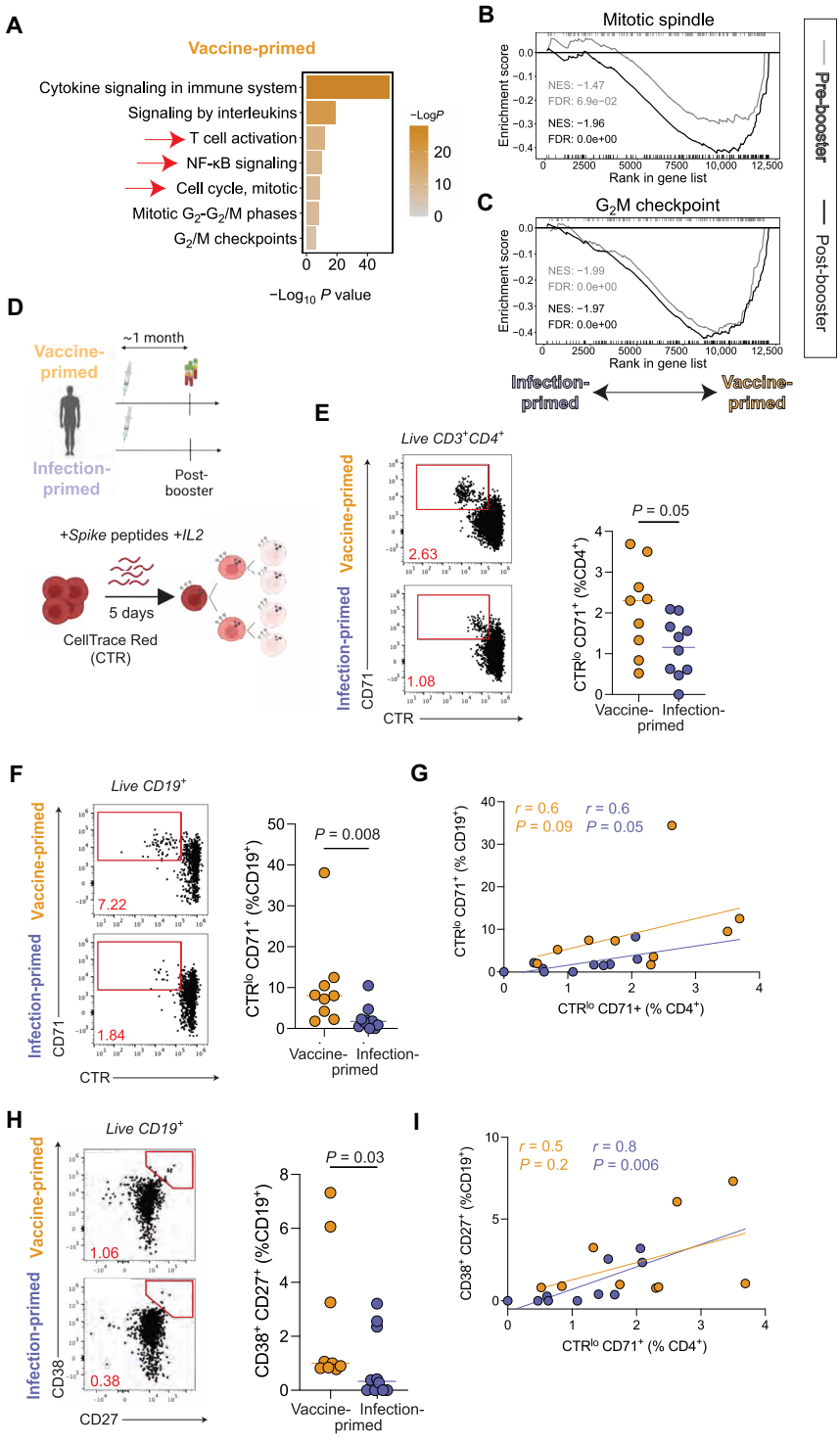

Fig. 7. Infection-primed transcriptional signature confers a proliferative disadvantage. (**A**) Gene ontology analysis for DEGs at $P_{adj} < 0.05$ for vaccine-primed S-specific CD4 T cells relative to infection-primed cells at post-booster time point. (**B** and **C**) GSEA for (B) mitotic spindle and (C) G_2M checkpoint gene sets for S-specific CD4 T cells. The light gray line indicates the pre-booster time point, and the dark gray line indicates the post-booster time point. Negative enrichment scores denote enrichment toward the vaccine-primed cohort. (**D**) Study schematic of in vitro proliferation experiments with vaccine-primed and infection-primed post-booster samples. PBMCs were stained with CTR and stimulated with S peptides and IL-2 for 5 days. (**E** and **F**) Representative flow cytometry plots and summary data for vaccine- ($n = 9$) and infection-primed ($n = 10$) participants for (E) CD4 T cells and (F) B cells post-booster for CD71 and CellTrace Red (CTR) after PBMC stimulation with S peptides. (**G**) Spearman correlation between frequency of $CTR^{lo}CD71^+$ CD4 T cells and $CTR^{lo}CD71^+$ $CD19^+$ cells. (**H**) Representative flow cytometry plots and summary data for expression of CD38 and CD27 in B cells from vaccine- ($n = 9$) and infection-primed ($n = 10$) participants after PBMC stimulation with S peptides. (**I**) Spearman correlation between frequency of $CTR^{lo}CD71^+$ CD4 T cells and $CD38^+CD27^+$ $CD19^+$ cells. Frequency shown in red and *P* values by Wilcoxon test in (E, F, and I). Vaccine-primed cohort points and correlation lines shown in orange and infection-primed cohort in purple for (G) and (I).

informed consent, peripheral blood was drawn by standard phlebotomy longitudinally from 24 adults (12 vaccine-primed and 12 infection-primed) in observational studies in accordance with New York University (NYU) Institutional Review Board protocols (s18-02035 and s18-02037) and previously described (*12*, *41*). Participant demographics are summarized in tables S1 to S3. Dates depicted in figs. S1A and S4A have been randomly offset to protect patient privacy (*75*).

Blood sample processing and storage

Blood draws occurred around 6 months after either vaccination ("postvaccination") or infection ("postinfection"), 8 months after second vaccination ("pre-booster"), and 1 month after third vaccination ("post-booster") (Figs. 1A and 4A). PBMCs were isolated from Cell Preparation Tube (CPT) Vacutainers (BD Biosciences) within 4 hours of the blood draw and cryopreserved.

AIM analysis

Cryopreserved PBMCs were thawed and rested overnight at 37°C in RPMI 1640 with L-glutamine (Thermo Fisher Scientific) containing 10% fetal bovine serum (FBS; Thermo Fisher Scientific) and 2 mM L-glutamine (Thermo Fisher Scientific) and supplemented with 10 U of deoxyribonuclease I (DNase I; New England BioLabs) and 5 mM $MgCl_2$ (Thermo Fisher Scientific). The following day, cells were stimulated with combined 15-nucleotide oligomer peptide pools encompassing the SARS-CoV-2 S protein (S1, S, and S^+ PepTivators, Miltenyi). Sterile water was used for the unstimulated controls. After stimulation for 20 hours at 37°C, cells were washed with phosphate-buffered saline containing 10 mM EDTA for 5 min before subsequent use.

Flow cytometry

Flow cytometry staining was performed using fluorescently labeled anti-human antibodies (table S4). Briefly, cells after AIM assay underwent Fc blockade at 1:100 with Human TruStain FcX (BioLegend) and NovaBlock (Thermo Fisher Scientific) for 10 min at room temperature, followed by surface antibody staining at room temperature for 20 min in the dark. Samples not planned for use in scRNA-seq were permeabilized using the eBioscience Foxp3/Transcription Factor Staining Buffer Set (Thermo Fisher Scientific) for 20 min at room temperature in the dark. After permeabilization, cells were intracellularly stained for 1 hour at room temperature in the dark, followed by resuspension in 1% paraformaldehyde (Electron Microscopy Sciences). All samples were acquired on a five-laser Aurora cytometer (Cytek Biosciences). Data were analyzed with FlowJo v.10.8.

Tetramer staining

PBMCs used for tetramer staining were thawed and rested overnight at 37°C in RPMI 1640 with L-glutamine (Thermo Fisher Scientific) containing 10% FBS (Thermo Fisher Scientific) and 2 mM L-glutamine (Thermo Fisher Scientific) and supplemented with DNase and $MgCl_2$. The following day, cells were stained with Fc blockade at 1:100 and BV421-labeled HLA-DPB1*04:01 $S_{167–180}$ tetramer (MBL International) at 1:20 for 2 hours at 37°C, followed by surface antibody staining, permeabilization, intracellular staining, and acquisition as described above.

Expanded cellular indexing of transcriptomes and epitopes by sequencing

After overnight stimulation in the AIM assay (above), cells were stained with antibodies against CD69 and CD137 conjugated to phycoerythrin (PE)–Dazzle594 and PE, respectively (BioLegend), for 30 min at room temperature in the dark, followed by magnetic bead enrichment using the EasySep Human PE Positive Selection Kit (STEMCELL Technologies) but with only a single decanting step. Cells were processed for exCITE-seq using the Chromium Next GEM Single Cell 5′ HT Kit v2 (10x Genomics). Cells were stained with hashtag oligos (BioLegend) as previously described (*45*, *76*–*78*). Cells were pooled and loaded onto Chromium HT Chips and run on a Chromium controller (10x Genomics). Gene expression, V(D)J, and surface protein expression libraries were made using the 5′ Feature Barcode Kit, Chromium Single Cell V(D)J Amplification Kit, and the Chromium Next GEM Single Cell 5′ Library Kit (10x Genomics) as recommended by the manufacturer. Libraries were pooled and sequenced using the NovaSeq 6000.

exCITE-seq data processing

Cellranger software v6.0.1 (10x Genomics) was used to align FASTQ files to the human genome (GRCh38 ensemble) and to perform protein expression evaluation. Seurat v4.3.0 (*46*) was used to process single-cell libraries and integrate all the exCITE-seq modalities. Empty droplets were excluded on the basis of the barcode-rank distribution. After CLR normalization, hashtag oligos (HTOs) were demultiplexed using the Seurat function HTODemux(). Cells were excluded on the basis of mitochondrial content of >8% or if the cell contained <400 or >7000 unique molecular identifier (UMI) counts. Doublets were identified using scDblFinder (*79*) on the basis of an estimated doublet rate of 0.4%. RNA was normalized across batches using SCTransform, and filtered counts were integrated in Seurat using SelectIntegrationFeatures() for 3000 features, followed by FindIntegrationAnchors() using the first 30 dimensions with "rpca" dimensionality reduction and k.anchors = 20. TCR sequences were processed and analyzed using scRepertoire v1.7.4 (*80*). SPICE was used to analyze polyfunctionality (version 6.1) (*81*). The following list of genes (*82*–*84*) was used to identify functional phenotypes in the S-reactive CD4 T cluster: *CCR4*, *CCR5*, *CCR6*, *CCR7*, *CXCR3*, *CXCR4*, *CXCR5 FOXP3*, *GATA3*, *IFNG*, *IL2*, *IL2RA*, *IL4*, *IL5*, *IL10*, *IL12A*, *IL13*, *IL17A*, *IL21*, *RORC*, *RUNX3*, *STAT3*, *STAT4*, *STAT6*, *TBX21*, *TGFB1*, and *TNF*. Gene ontology was performed using Metascape (*85*). Differential expression analysis was performed using DESeq2 v1.34.0 (*86*) after filtering for genes with at least 10 counts in at least three samples. Preranked GSEA was performed with 10,000 permutations of gene sets from the Molecular Signatures Database (MSigDB) (*87*).

Transcriptomic, epitope, and accessibility by sequencing

After overnight stimulation in the AIM assay (above), CD4 T cells were isolated using the EasySep Human CD4 T Cell Isolation Kit (STEMCELL Technologies). Next, isolated CD4 T cells were stained with antibodies against CD69 and CD137 conjugated to PE-Dazzle594 and PE, respectively (BioLegend), and with hashtag oligos (BioLegend) for 30 min at room temperature in the dark, followed by magnetic bead enrichment using the EasySep Human PE Positive Selection Kit (STEMCELL Technologies). Cells were then processed for transcriptomic, epitope, and accessibility measurement (TEA-seq) (*55*) using the Chromium Next GEM Single Cell Multiome ATAC + Gene Expression Kit (10x Genomics). Cells were pooled and loaded onto Chromium J Chips and run on a Chromium X controller (10x Genomics). Gene expression and ATAC libraries were made using the Chromium Next GEM Single Cell Multiome ATAC Kit A, Chromium Next GEM Single Cell Multiome Reagent Kit A, and Library Construction Kit (10x Genomics) following the protocols recommended by the manufacturer. Surface protein expression libraries were made as detailed in the TEA-seq protocol. Libraries were pooled at desired concentrations and sequenced using the NovaSeq 6000.

TEA-seq data processing

RNA and ATAC libraries were aligned using cellranger-arc v1.2.0 (10x Genomics) against the human genome (GRCh38 ensemble). Primary data analysis and statistical analysis were then performed using the R environment. BarCounter (*55*), Seurat v4.3.0 (*46*), and Signac v1.9.0 (*88*) were used to process single-cell libraries and integrate all the TEA-seq modalities. HTOs were demultiplexed using HTODemux(), and scDblFinder identified doublets (*79*) on the basis of an estimated doublet rate of 0.8%. RNA was normalized across batches using the

same integration methods applied to exCITE-seq data. Preranked GSEA was performed with 10,000 permutations of gene sets from the MSigDB. To create a merged peak list as originally called by cellranger-arc, OCRs were normalized across batches in Seurat using IntegrateEmbeddings(). Subsetting down to the S-reactive CD4 T cluster, peaks were recalled using MACS2 (*89*). Differential accessibility was performed using the Seurat FindMarkers() function with test.use = "LR." We identified peaks which contained DNA motifs that were present in the JASPAR database for humans (*90*). The Signac library's FindMotifs() function was used to identify overrepresented motifs in the top DARs in each cohort (nominal $P < 0.005$) compared with background, matched for overall GC content. ChEA3 (*64*) was used to predict TF activity associated with input gene lists (data S1).

S peptide proliferation assay

Thawed and rested PBMCs were first labeled with the CellTrace Far Red Proliferation Kit (0.5 μM, Thermo Fisher Scientific). Because frequencies of S-specific CD4 T cells were similar between cohorts (fig. S1E), PBMCs were used directly without enrichment or isolation of antigen-specific CD4 T cells. Then, 1×10^6 PBMCs in AIM V Medium (Thermo Fisher Scientific) were stimulated with 15-nucleotide oligomer peptide pools encompassing the SARS-CoV-2 S protein (S1, S, and S^+ PepTivators, Miltenyi) in a 96-well flat-bottom plate for 5 days at 37°C in the presence of recombinant IL-2 (100 IU/ml; BioLegend). As a positive control, cells were cultured with staphylococcal enterotoxin B (Toxin Technologies) (50 ng/ml) and recombinant human IL-2 (100 IU/ml). As an unstimulated control, cells were cultured with rIL-2 and sterile water in AIM V Medium. After stimulation, flow cytometry was performed as described above.

Statistics

Nonparametric tests were preferentially used throughout using two-tailed tests at $\alpha = 0.05$, unless otherwise indicated. Where paired analyses were performed, the unpaired data points were excluded. Outlier analysis was not performed, and, thus, outliers were not excluded from the primary analyses. Genes were considered differentially expressed at a false discovery rate (FDR) ≤ 0.05. Prism 9.0 and R were used to perform statistical analyses. Study schematics were made using BioRender.

Supplementary Materials

This PDF file includes:
Figs. S1 to S7
Tables S1 to S4

Other Supplementary Material for this manuscript includes the following:
Data files S1 to S7
MDAR Reproducibility Checklist

REFERENCES AND NOTES

1. S. Adamo, J. Michler, Y. Zurbuchen, C. Cervia, P. Taeschler, M. E. Raeber, S. Baghai Sain, J. Nilsson, A. E. Moor, O. Boyman, Signature of long-lived memory $CD8^+$ T cells in acute SARS-CoV-2 infection. *Nature* **602**, 148–155 (2022).
2. A. T. Tan, M. Linster, C. W. Tan, N. Le Bert, W. N. Chia, K. Kunasegaran, Y. Zhuang, C. Y. L. Tham, A. Chia, G. J. D. Smith, B. Young, S. Kalimuddin, J. G. H. Low, D. Lye, L.-F. Wang, A. Bertoletti, Early induction of functional SARS-CoV-2-specific T cells associates with rapid viral clearance and mild disease in COVID-19 patients. *Cell Rep.* **34**, 108728 (2021).
3. S. A. Plotkin, Updates on immunologic correlates of vaccine-induced protection. *Vaccine* **38**, 2250–2257 (2020).
4. T. C. Wirth, M. D. Martin, G. Starbeck-Miller, J. T. Harty, V. P. Badovinac, Secondary $CD8^+$ T-cell responses are controlled by systemic inflammation. *Eur. J. Immunol.* **41**, 1321–1333 (2011).
5. T. C. Wirth, J. T. Harty, V. P. Badovinac, Modulating numbers and phenotype of $CD8^+$ T cells in secondary immune responses. *Eur. J. Immunol.* **40**, 1916–1926 (2010).
6. K. B. Pruner, M. Pepper, Local memory CD4 T cell niches in respiratory viral infection. *J. Exp. Med.* **218**, e20201733 (2021).
7. B. J. Laidlaw, J. E. Craft, S. M. Kaech, The multifaceted role of $CD4^+$ T cells in $CD8^+$ T cell memory. *Nat. Rev. Immunol.* **16**, 102–111 (2016).
8. T. M. Wilkinson, C. K. F. Li, C. S. C. Chui, A. K. Y. Huang, M. Perkins, J. C. Liebner, R. Lambkin-Williams, A. Gilbert, J. Oxford, B. Nicholas, K. J. Staples, T. Dong, D. C. Douek, A. J. McMichael, X.-N. Xu, Preexisting influenza-specific $CD4^+$ T cells correlate with disease protection against influenza challenge in humans. *Nat. Med.* **18**, 274–280 (2012).
9. J. Zhao, J. Zhao, A. K. Mangalam, R. Channappanavar, C. Fett, D. K. Meyerholz, S. Agnihothram, R. S. Baric, C. S. David, S. Perlman, Airway memory $CD4^+$ T cells mediate protective immunity against emerging respiratory coronaviruses. *Immunity* **44**, 1379–1391 (2016).
10. E. Panagioti, P. Klenerman, L. N. Lee, S. H. van der Burg, R. Arens, Features of effective T cell-inducing vaccines against chronic viral infections. *Front. Immunol.* **9**, 276 (2018).
11. N. J. Tubo, M. K. Jenkins, TCR signal quantity and quality in $CD4^+$ T cell differentiation. *Trends Immunol.* **35**, 591–596 (2014).
12. M. I. Samanovic, A. R. Cornelius, S. L. Gray-Gaillard, J. R. Allen, T. Karmacharya, J. P. Wilson, S. W. Hyman, M. Tuen, S. B. Koralov, M. J. Mulligan, R. S. Herati, Robust immune responses are observed after one dose of BNT162b2 mRNA vaccine dose in SARS-CoV-2-experienced individuals. *Sci. Transl. Med.* **14**, eabi8961 (2022).
13. L. B. Rodda, P. A. Morawski, K. B. Pruner, M. L. Fahning, C. A. Howard, N. Franko, J. Logue, J. Eggenberger, C. Stokes, I. Golez, M. Hale, M. Gale Jr., H. Y. Chu, D. J. Campbell, M. Pepper, Imprinted SARS-CoV-2-specific memory lymphocytes define hybrid immunity. *Cell* **185**, 1588–1601.e14 (2022).
14. R. W. Nelson, Y. Chen, O. L. Venezia, R. M. Majerus, D. S. Shin, D. R. Wesemann, MGH COVID-19 Collection & Processing Team, M. N. Carrington, X. G. Yu, D. R. Wesemann, J. J. Moon, A. D. Luster, SARS-CoV-2 epitope-specific $CD4^+$ memory T cell responses across COVID-19 disease severity and antibody durability. *Sci. Immunol.* **7**, eabl9464 (2022).
15. R. R. Goel, M. M. Painter, S. A. Apostolidis, D. Mathew, W. Meng, A. M. Rosenfeld, K. A. Lundgreen, A. Reynaldi, D. S. Khoury, A. Pattekar, S. Gouma, L. Kuri-Cervantes, P. Hicks, S. Dysinger, A. Hicks, H. Sharma, S. Herring, S. Korte, A. E. Baxter, D. A. Oldridge, J. R. Giles, M. E. Weirick, C. M. McAllister, M. Awofolaju, N. Tanenbaum, E. M. Drapeau, J. Dougherty, S. Long, K. D'Andrea, J. T. Hamilton, M. McLaughlin, J. C. Williams, S. Adamski, O. Kuthuru, UPenn COVID Processing Unit, I. Frank, M. R. Betts, L. A. Vella, A. Grifoni, D. Weiskopf, A. Sette, S. E. Hensley, M. P. Davenport, P. Bates, E. T. L. Prak, A. R. Greenplate, E. J. Wherry, mRNA vaccines induce durable immune memory to SARS-CoV-2 and variants of concern. *Science* **374**, abm0829 (2021).
16. J. M. Dan, J. Mateus, Y. Kato, K. M. Hastie, E. D. Yu, C. E. Faliti, A. Grifoni, S. I. Ramirez, S. Haupt, A. Frazier, C. Nakao, V. Rayaprolu, S. A. Rawlings, B. Peters, F. Krammer, V. Simon, E. O. Saphire, D. M. Smith, D. Weiskopf, A. Sette, S. Crotty, Immunological memory to SARS-CoV-2 assessed for up to 8 months after infection. *Science* **371**, eabf4063 (2021).
17. U. Sahin, A. Muik, E. Derhovanessian, I. Vogler, L. M. Kranz, M. Vormehr, A. Baum, K. Pascal, J. Quandt, D. Maurus, S. Brachtendorf, V. Lörks, J. Sikorski, R. Hilker, D. Becker, A.-K. Eller, J. Grützner, C. Boesler, C. Rosenbaum, M.-C. Kühnle, U. Luxemburger, A. Kemmer-Brück, D. Langer, M. Bexon, S. Bolte, K. Karikó, T. Palanche, B. Fischer, A. Schultz, P.-Y. Shi, C. Fontes-Garfias, J. L. Perez, K. A. Swanson, J. Loschko, I. L. Scully, M. Cutler, W. Kalina, C. A. Kyratsous, D. Cooper, P. R. Dormitzer, K. U. Jansen, Ö. Türeci, COVID-19 vaccine BNT162b1 elicits human antibody and TH1 T cell responses. *Nature* **586**, 594–599 (2020).
18. M. M. Painter, D. Mathew, R. R. Goel, S. A. Apostolidis, A. Pattekar, O. Kuthuru, A. E. Baxter, R. S. Herati, D. A. Oldridge, S. Gouma, P. Hicks, S. Dysinger, K. A. Lundgreen, L. Kuri-Cervantes, S. Adamski, A. Hicks, S. Korte, J. R. Giles, M. E. Weirick, C. M. McAllister, J. Dougherty, S. Long, K. D'Andrea, J. T. Hamilton, M. R. Betts, P. Bates, S. E. Hensley, A. Grifoni, D. Weiskopf, A. Sette, A. R. Greenplate, E. J. Wherry, Rapid induction of antigen-specific $CD4^+$ T cells is associated with coordinated humoral and cellular immunity to SARS-CoV-2 mRNA vaccination. *Immunity* **54**, 2133–2142.e3 (2021).
19. M. Koutsakos, A. Reynaldi, W. S. Lee, J. Nguyen, T. Amarasena, G. Taiaroa, P. Kinsella, K. C. Liew, T. Tran, H. E. Kent, H.-X. Tan, L. C. Rowntree, T. H. O. Nguyen, P. G. Thomas, K. Kedzierska, J. Petersen, J. Rossjohn, D. A. Williamson, D. Khoury, M. P. Davenport, S. J. Kent, A. K. Wheatley, J. A. Juno, SARS-CoV-2 breakthrough infection induces rapid memory and de novo T cell responses. *Immunity* **56**, 879–892.e4 (2023).
20. M. M. Painter, T. S. Johnston, K. A. Lundgreen, J. J. S. Santos, J. S. Qin, R. R. Goel, S. A. Apostolidis, D. Mathew, B. Fulmer, J. C. Williams, M. L. McKeague, A. Pattekar, A. Goode, S. Nasta, A. E. Baxter, J. R. Giles, A. N. Skelly, L. E. Felley, M. McLaughlin, J. Weaver; Penn Medicine BioBank, O. Kuthuru, J. Dougherty, S. Adamski, S. Long, M. Kee, C. Clendenin, R. da Silva Antunes, A. Grifoni, D. Weiskopf, A. Sette, A. C. Huang, D. J. Rader, S. E. Hensley, P. Bates, A. R. Greenplate, E. J. Wherry, Prior vaccination enhances immune responses during SARS-CoV-2 breakthrough

infection with early activation of memory T cells followed by production of potent neutralizing antibodies. bioRxiv 527215 [Preprint] (2023). https://doi.org/10.1101/2023.02.05.527215.
21. S. Keck, M. Schmaler, S. Ganter, L. Wyss, S. Oberle, E. S. Huseby, D. Zehn, C. G. King, Antigen affinity and antigen dose exert distinct influences on CD4 T-cell differentiation. *Proc. Natl. Acad. Sci. U.S.A.* **111**, 14852–14857 (2014).
22. D. J. Shedlock, H. Shen, Requirement for CD4 T cell help in generating functional CD8 T cell memory. *Science* **300**, 337–339 (2003).
23. E. N. Ivanova, J. Shwetar, J. C. Devlin, T. B. Buus, S. Gray-Gaillard, A. Koide, A. Cornelius, M. I. Samanovic, A. Herrera, E. P. Mimitou, C. Zhang, T. Karmacharya, L. Desvignes, N. Ødum, P. Smibert, R. J. Ulrich, M. J. Mulligan, S. Koide, K. V. Ruggles, R. S. Herati, S. B. Koralov, mRNA COVID-19 vaccine elicits potent adaptive immune response without the acute inflammation of SARS-CoV-2 infection. *iScience* **26**, 108572 (2023).
24. M. Merad, J. C. Martin, Pathological inflammation in patients with COVID-19: A key role for monocytes and macrophages. *Nat. Rev. Immunol.* **20**, 355–362 (2020).
25. R. S. Thwaites, A. Sanchez Sevilla Uruchurtu, M. K. Siggins, F. Liew, C. D. Russell, S. C. Moore, C. Fairfield, E. Carter, S. Abrams, C.-E. Short, T. Thaventhiran, E. Bergstrom, Z. Gardener, S. Ascough, C. Chiu, A. B. Docherty, D. Hunt, Y. J. Crow, T. Solomon, G. P. Taylor, L. Turtle, E. M. Harrison, J. Dunning, M. G. Semple, J. K. Baillie, P. J. Openshaw, ISARIC4C investigators, Inflammatory profiles across the spectrum of disease reveal a distinct role for GM-CSF in severe COVID-19. *Sci Immunol.* **6**, eabg9873 (2021).
26. P. S. Arunachalam, F. Wimmers, C. K. P. Mok, R. A. P. M. Perera, M. Scott, T. Hagan, N. Sigal, Y. Feng, L. Bristow, O. Tak-Yin Tsang, D. Wagh, J. Coller, K. L. Pellegrini, D. Kazmin, G. Alaaeddine, W. S. Leung, J. M. C. Chan, T. S. H. Chik, C. Y. C. Choi, C. Huerta, M. Paine McCullough, H. Lv, E. Anderson, S. Edupuganti, A. A. Upadhyay, S. E. Bosinger, H. T. Maecker, P. Khatri, N. Rouphael, M. Peiris, B. Pulendran, Systems biological assessment of immunity to mild versus severe COVID-19 infection in humans. *Science* **369**, 1210–1220 (2020).
27. P. S. Arunachalam, M. K. D. Scott, T. Hagan, C. Li, Y. Feng, F. Wimmers, L. Grigoryan, M. Trisal, V. V. Edara, L. Lai, S. E. Chang, A. Feng, S. Dhingra, M. Shah, A. S. Lee, S. Chinthrajah, S. B. Sindher, V. Mallajosyula, F. Gao, N. Sigal, S. Kowli, S. Gupta, K. Pellegrini, G. Tharp, S. Maysel-Auslender, S. Hamilton, H. Aoued, K. Hrusovsky, M. Roskey, S. E. Bosinger, H. T. Maecker, S. D. Boyd, M. M. Davis, P. J. Utz, M. S. Suthar, P. Khatri, K. C. Nadeau, B. Pulendran, Systems vaccinology of the BNT162b2 mRNA vaccine in humans. *Nature* **596**, 410–416 (2021).
28. E. E. Walsh, R. W. Frenck Jr., A. R. Falsey, N. Kitchin, J. Absalon, A. Gurtman, S. Lockhart, K. Neuzil, M. J. Mulligan, R. Bailey, K. A. Swanson, P. Li, K. Koury, W. Kalina, D. Cooper, C. Fontes-Garfias, P.-Y. Shi, Ö. Türeci, K. R. Tompkins, K. E. Lyke, V. Raabe, P. R. Dormitzer, K. U. Jansen, U. Şahin, W. C. Gruber, Safety and immunogenicity of two RNA-based covid-19 vaccine candidates. *N. Engl. J. Med.* **383**, 2439–2450 (2020).
29. L. R. Baden, H. M. El Sahly, B. Essink, K. Kotloff, S. Frey, R. Novak, D. Diemert, S. A. Spector, N. Rouphael, C. B. Creech, J. McGettigan, S. Khetan, N. Segall, J. Solis, A. Brosz, C. Fierro, H. Schwartz, K. Neuzil, L. Corey, P. Gilbert, H. Janes, D. Follmann, M. Marovich, J. Mascola, L. Polakowski, J. Ledgerwood, B. S. Graham, H. Bennett, R. Pajon, C. Knightly, B. Leav, W. Deng, H. Zhou, S. Han, M. Ivarsson, J. Miller, T. Zaks, Efficacy and safety of the mRNA-1273 SARS-CoV-2 vaccine. *N. Engl. J. Med.* **384**, 403–416 (2021).
30. F. P. Polack, S. J. Thomas, N. Kitchin, J. Absalon, A. Gurtman, S. Lockhart, J. L. Perez, G. Pérez Marc, E. D. Moreira, C. Zerbini, R. Bailey, K. A. Swanson, S. Roychoudhury, K. Koury, P. Li, W. V. Kalina, D. Cooper, R. W. Frenck Jr., L. L. Hammitt, Ö. Türeci, H. Nell, A. Schaefer, S. Ünal, D. B. Tresnan, S. Mather, P. R. Dormitzer, U. Şahin, K. U. Jansen, W. C. Gruber, C4591001 Clinical Trial Group, Safety and efficacy of the BNT162b2 mRNA Covid-19 vaccine. *N. Engl. J. Med.* **383**, 2603–2615 (2020).
31. M. D. Martin, V. P. Badovinac, T. S. Griffith, CD4 T cell responses and the sepsis-induced immunoparalysis state. *Front. Immunol.* **11**, 1364 (2020).
32. I. J. Jensen, X. Li, P. W. McGonagill, Q. Shan, M. G. Fosdick, M. M. Tremblay, J. C. Houtman, H.-H. Xue, T. S. Griffith, W. Peng, V. P. Badovinac, Sepsis leads to lasting changes in phenotype and function of memory CD8 T cells. *eLife* **10**, e70989 (2021).
33. S. J. Moioffer, D. B. Danahy, S. van de Wall, I. J. Jensen, F. V. Sjaastad, S. M. Anthony, J. T. Harty, T. S. Griffith, V. P. Badovinac, Severity of sepsis determines the degree of impairment observed in circulatory and tissue-resident memory CD8 T cell populations. *J. Immunol.* **207**, 1871–1881 (2021).
34. M. I. Samanovic, A. L. Oom, A. R. Cornelius, S. L. Gray-Gaillard, T. Karmacharya, M. Tuen, J. P. Wilson, M. F. Tasissa, S. Goins, R. S. Herati, M. J. Mulligan, Vaccine-acquired SARS-CoV-2 immunity versus infection-acquired immunity: A comparison of three COVID-19 vaccines. *Vaccines* **10**, 2152 (2022).
35. R. S. Herati, A. Muselman, L. Vella, B. Bengsch, K. Parkhouse, D. Del Alcazar, J. Kotzin, S. A. Doyle, P. Tebas, S. E. Hensley, L. F. Su, K. E. Schmader, E. J. Wherry, Successive annual influenza vaccination induces a recurrent oligoclonotypic memory response in circulating T follicular helper cells. *Sci Immunol.* **2**, eaag2152 (2017).
36. A. Grifoni, D. Weiskopf, S. I. Ramirez, J. Mateus, J. M. Dan, C. R. Moderbacher, S. A. Rawlings, A. Sutherland, L. Premkumar, R. S. Jadi, D. Marrama, A. M. de Silva, A. Frazier, A. F. Carlin, J. A. Greenbaum, B. Peters, F. Krammer, D. M. Smith, S. Crotty, A. Sette, Targets of T cell responses to SARS-CoV-2 coronavirus in humans with COVID-19 disease and unexposed individuals. *Cell* **181**, 1489–1501.e15 (2020).
37. J. M. Dan, C. S. Lindestam Arlehamn, D. Weiskopf, R. da Silva Antunes, C. Havenar-Daughton, S. M. Reiss, M. Brigger, M. Bothwell, A. Sette, S. Crotty, A cytokine-independent approach to identify antigen-specific human germinal center T follicular helper cells and rare antigen-specific $CD4^+$ T cells in blood. *J. Immunol.* **197**, 983–993 (2016).
38. C. Havenar-Daughton, S. M. Reiss, D. G. Carnathan, J. E. Wu, K. Kendric, A. T. de la Peña, S. P. Kasturi, J. M. Dan, M. Bothwell, R. W. Sanders, B. Pulendran, G. Silvestri, S. Crotty, Cytokine-independent detection of antigen-specific germinal center T follicular helper cells in immunized nonhuman primates using a live cell activation-induced marker technique. *J. Immunol.* **197**, 994–1002 (2016).
39. P. A. Mudd, A. A. Minervina, M. V. Pogorelyy, J. S. Turner, W. Kim, E. Kalaidina, J. Petersen, A. J. Schmitz, T. Lei, A. Haile, A. M. Kirk, R. C. Mettelman, J. C. Crawford, T. H. O. Nguyen, L. C. Rowntree, E. Rosati, K. A. Richards, A. J. Sant, M. K. Klebert, T. Suessen, W. D. Middleton, SJTRC Study Team, J. Wolf, S. A. Teefey, J. A. O'Halloran, R. M. Presti, K. Kedzierska, J. Rossjohn, P. G. Thomas, A. H. Ellebedy, SARS-CoV-2 mRNA vaccination elicits a robust and persistent T follicular helper cell response in humans. *Cell* **185**, 603–613.e15 (2022).
40. F. Gao, V. Mallajoysula, P. S. Arunachalam, K. van der Ploeg, M. Manohar, K. Röltgen, F. Yang, O. Wirz, R. Hoh, E. Haraguchi, J.-Y. Lee, R. Willis, V. Ramachandiran, J. Li, K. R. Kathuria, C. Li, A. S. Lee, M. M. Shah, S. B. Sindher, J. Gonzalez, J. D. Altman, T. T. Wang, S. D. Boyd, B. Pulendran, P. Jagannathan, K. C. Nadeau, M. M. Davis, Spheromers reveal Robust T cell responses to the Pfizer/BioNTech vaccine and attenuated peripheral $CD8^+$ T cell responses post SARS-CoV-2 infection. *Immunity* **56**, 864–878.e4 (2023).
41. C. J. Reynolds, C. Pade, J. M. Gibbons, A. D. Otter, K.-M. Lin, D. Muñoz Sandoval, F. P. Pieper, D. K. Butler, S. Liu, G. Joy, N. Forooghi, T. A. Treibel, C. Manisty, J. C. Moon, COVIDsortium Investigators, COVIDsortium Immune Correlates Network, A. Semper, T. Brooks, Á. McKnight, D. M. Altmann, R. J. Boyton, Immune boosting by B.1.1.529 (Omicron) depends on previous SARS-CoV-2 exposure. *Science* **377**, eabq1841 (2022).
42. S. Reiss, A. E. Baxter, K. M. Cirelli, J. M. Dan, A. Morou, A. Daigneault, N. Brassard, G. Silvestri, J.-P. Routy, C. Havenar-Daughton, S. Crotty, D. E. Kaufmann, Comparative analysis of activation induced marker (AIM) assays for sensitive identification of antigen-specific CD4 T cells. *PLOS ONE* **12**, e0186998 (2017).
43. V. Naranbhai, A. Nathan, C. Kaseke, C. Berrios, A. Khatri, S. Choi, M. A. Getz, R. Tano-Menka, O. Ofoman, A. Gayton, F. Senjobe, Z. Zhao, K. J. St Denis, E. C. Lam, M. Carrington, W. F. Garcia-Beltran, A. B. Balazs, B. D. Walker, A. J. Iafrate, G. D. Gaiha, T cell reactivity to the SARS-CoV-2 Omicron variant is preserved in most but not all individuals. *Cell* **185**, 1041–1051.e6 (2022).
44. K. M. Wragg, W. S. Lee, M. Koutsakos, H.-X. Tan, T. Amarasena, A. Reynaldi, G. Gare, P. Konstandopoulos, K. R. Field, R. Esterbauer, H. E. Kent, M. P. Davenport, A. K. Wheatley, S. J. Kent, J. A. Juno, Establishment and recall of SARS-CoV-2 spike epitope-specific $CD4^+$ T cell memory. *Nat. Immunol.* **23**, 768–780 (2022).
45. E. P. Mimitou, A. Cheng, A. Montalbano, S. Hao, M. Stoeckius, M. Legut, T. Roush, A. Herrera, E. Papalexi, Z. Ouyang, R. Satija, N. E. Sanjana, S. B. Koralov, P. Smibert, Multiplexed detection of proteins, transcriptomes, clonotypes and CRISPR perturbations in single cells. *Nat. Methods* **16**, 409–412 (2019).
46. Y. Hao, S. Hao, E. Andersen-Nissen, W. M. Mauck III, S. Zheng, A. Butler, M. J. Lee, A. J. Wilk, C. Darby, M. Zager, P. Hoffman, M. Stoeckius, E. Papalexi, E. P. Mimitou, J. Jain, A. Srivastava, T. Stuart, L. M. Fleming, B. Yeung, A. J. Rogers, J. M. McElrath, C. A. Blish, R. Gottardo, P. Smibert, R. Satija, Integrated analysis of multimodal single-cell data. *Cell* **184**, 3573–3587.e29 (2021).
47. S. Nolan, M. Vignali, M. Klinger, J. N. Dines, I. M. Kaplan, E. Svejnoha, T. Craft, K. Boland, M. Pesesky, R. M. Gittelman, T. M. Snyder, C. J. Gooley, S. Semprini, C. Cerchione, M. Mazza, O. M. Delmonte, K. Dobbs, G. Carreño-Tarragona, S. Barrio, V. Sambri, G. Martinelli, J. D. Goldman, J. R. Heath, L. D. Notarangelo, J. M. Carlson, J. Martinez-Lopez, H. S. Robins, A large-scale database of T-cell receptor beta (TCRβ) sequences and binding associations from natural and synthetic exposure to SARS-CoV-2, Research Square [preprint] (2021); https://www.researchsquare.com/article/rs-51964/v1.
48. G. Guerrera, M. Picozza, S. D'Orso, R. Placido, M. Pirronello, A. Verdiani, A. Termine, C. Fabrizio, F. Giannessi, M. Sambucci, M. P. Balice, C. Caltagirone, A. Salvia, A. Rossini, L. Battistini, G. Borsellino, BNT162b2 vaccination induces durable SARS-CoV-2–specific T cells with a stem cell memory phenotype. *Sci. Immunol.* **6**, eabl5344 (2021).
49. A. Paolini, R. Borella, A. Neroni, D. Lo Tartaro, M. Mattioli, L. Fidanza, A. Di Nella, E. Santacroce, L. Gozzi, S. Busani, T. Trenti, M. Meschiari, G. Guaraldi, M. Girardis, C. Mussini, L. Gibellini, S. De Biasi, A. Cossarizza, Patients recovering from severe COVID-19 develop a polyfunctional antigen-specific $CD4^+$ T cell response. *Int. J. Mol. Sci.* **23**, 8004 (2022).
50. E. Ivanova, J. Devlin, T. Buus, A. Koide, A. Cornelius, M. Samanovic, A. Herrera, C. Zhang, L. Desvignes, N. Odum, R. Ulrich, M. J. Mulligan, S. Koide, K. V. Ruggles, R. Herati, S. B. Koralov, Discrete immune response signature to SARS-CoV-2 mRNA vaccination versus infection, SSRN [preprint] (2021); https://ssrn.com/abstract=3838993.

51. Q. Xu, P. Milanez-Almeida, A. J. Martins, A. J. Radtke, K. B. Hoehn, C. Oguz, J. Chen, C. Liu, J. Tang, G. Grubbs, S. Stein, S. Ramelli, J. Kabat, H. Behzadpour, M. Karkanitsa, J. Spathies, H. Kalish, L. Kardava, M. Kirby, F. Cheung, S. Preite, P. C. Duncker, M. M. Kitakule, N. Romero, D. Preciado, L. Gitman, G. Koroleva, G. Smith, A. Shaffer, I. T. McBain, P. J. McGuire, S. Pittaluga, R. N. Germain, R. Apps, D. M. Schwartz, K. Sadtler, S. Moir, D. S. Chertow, S. H. Kleinstein, S. Khurana, J. S. Tsang, P. Mudd, P. L. Schwartzberg, K. Manthiram, Adaptive immune responses to SARS-CoV-2 persist in the pharyngeal lymphoid tissue of children. *Nat. Immunol.* **24**, 186–199 (2023).
52. B. J. Meckiff, C. Ramírez-Suástegui, V. Fajardo, S. J. Chee, A. Kusnadi, H. Simon, S. Eschweiler, A. Grifoni, E. Pelosi, D. Weiskopf, A. Sette, F. Ay, G. Seumois, C. H. Ottensmeier, P. Vijayanand, Imbalance of regulatory and cytotoxic SARS-CoV-2-reactive CD4$^+$ T cells in COVID-19. *Cell* **183**, 1340–1353.e16 (2020).
53. J. W. Schoggins, Interferon-stimulated genes: What do they all do? *Annu. Rev. Virol.* **6**, 567–584 (2019).
54. A. Subramanian, P. Tamayo, V. K. Mootha, S. Mukherjee, B. L. Ebert, M. A. Gillette, A. Paulovich, S. L. Pomeroy, T. R. Golub, E. S. Lander, J. P. Mesirov, Gene set enrichment analysis: A knowledge-based approach for interpreting genome-wide expression profiles. *Proc. Natl. Acad. Sci. U.S.A.* **102**, 15545–15550 (2005).
55. E. Swanson, C. Lord, J. Reading, A. T. Heubeck, P. C. Genge, Z. Thomson, M. D. A. Weiss, X.-J. Li, A. K. Savage, R. R. Green, T. R. Torgerson, T. F. Bumol, L. T. Graybuck, P. J. Skene, Simultaneous trimodal single-cell measurement of transcripts, epitopes, and chromatin accessibility using TEA-seq. *eLife* **10**, e63632 (2021).
56. C. Helbig, R. Gentek, R. A. Backer, Y. de Souza, I. A. M. Derks, E. Eldering, K. Wagner, D. Jankovic, T. Gridley, P. D. Moerland, R. A. Flavell, D. Amsen, Notch controls the magnitude of T helper cell responses by promoting cellular longevity. *Proc. Natl. Acad. Sci. U.S.A.* **109**, 9041–9046 (2012).
57. A. B. Wilkens, E. C. Fulton, M. J. Pont, G. O. Cole, I. Leung, S. M. Stull, M. R. Hart, I. D. Bernstein, S. N. Furlan, S. R. Riddell, NOTCH1 signaling during CD4$^+$ T-cell activation alters transcription factor networks and enhances antigen responsiveness. *Blood* **140**, 2261–2275 (2022).
58. K. Tomita, M. Hattori, E. Nakamura, S. Nakanishi, N. Minato, R. Kageyama, The bHLH gene Hes1 is essential for expansion of early T cell precursors. *Genes Dev.* **13**, 1203–1210 (1999).
59. M. E. De Obaldia, J. J. Bell, X. Wang, C. Harly, Y. Yashiro-Ohtani, J. H. DeLong, D. A. Zlotoff, D. A. Sultana, W. S. Pear, A. Bhandoola, T cell development requires constraint of the myeloid regulator C/EBP-α by the Notch target and transcriptional repressor Hes1. *Nat. Immunol.* **14**, 1277–1284 (2013).
60. R. Zhang, K. Chen, L. Peng, H. Xiong, Regulation of T helper cell differentiation by interferon regulatory factor family members. *Immunol. Res.* **54**, 169–176 (2012).
61. M. Lohoff, T. W. Mak, Roles of interferon-regulatory factors in T-helper-cell differentiation. *Nat. Rev. Immunol.* **5**, 125–135 (2005).
62. V. Krishnamoorthy, S. Kannanganat, M. Maienschein-Cline, S. L. Cook, J. Chen, N. Bahroos, E. Sievert, E. Corse, A. Chong, R. Sciammas, The IRF4 gene regulatory module functions as a read-write integrator to dynamically coordinate T helper cell fate. *Immunity* **47**, 481–497.e7 (2017).
63. V. Staudt, E. Bothur, M. Klein, K. Lingnau, S. Reuter, N. Grebe, B. Gerlitzki, M. Hoffmann, A. Ulges, C. Taube, N. Dehzad, M. Becker, M. Stassen, A. Steinborn, M. Lohoff, H. Schild, E. Schmitt, T. Bopp, Interferon-regulatory factor 4 is essential for the developmental program of T helper 9 cells. *Immunity* **33**, 192–202 (2010).
64. A. B. Keenan, D. Torre, A. Lachmann, A. K. Leong, M. L. Wojciechowicz, V. Utti, K. M. Jagodnik, E. Kropiwnicki, Z. Wang, A. Ma'ayan, ChEA3: Transcription factor enrichment analysis by orthogonal omics integration. *Nucleic Acids Res.* **47**, W212–W224 (2019).
65. S. Hänzelmann, R. Castelo, J. Guinney, GSVA: Gene set variation analysis for microarray and RNA-seq data. *BMC Bioinformatics* **14**, 7 (2013).
66. A. Ansari, S. Sachan, B. P. Jit, A. Sharma, P. Coshic, A. Sette, D. Weiskopf, N. Gupta, An efficient immunoassay for the B cell help function of SARS-CoV-2-specific memory CD4$^+$ T cells. *Cell Rep. Methods* **2**, 100224 (2022).
67. M. D. Galbraith, K. T. Kinning, K. D. Sullivan, P. Araya, K. P. Smith, R. E. Granrath, J. R. Shaw, R. Baxter, K. R. Jordan, S. Russell, M. Dzieciatkowska, J. A. Reisz, F. Gamboni, F. Cendali, T. Ghosh, K. Guo, C. C. Wilson, M. L. Santiago, A. A. Monte, T. D. Bennett, K. C. Hansen, E. W. Y. Hsieh, A. D'Alessandro, J. M. Espinosa, Specialized interferon action in COVID-19. *Proc. Natl. Acad. Sci. U.S.A.* **119**, e2116730119 (2022).
68. J. M. Amrute, A. M. Perry, G. Anand, C. Cruchaga, K. G. Hock, C. W. Farnsworth, G. J. Randolph, K. J. Lavine, A. L. Steed, Cell specific peripheral immune responses predict survival in critical COVID-19 patients. *Nat. Commun.* **13**, 882 (2022).
69. P. Laurent, C. Yang, A. F. Rendeiro, B. E. Nilsson-Payant, L. Carrau, V. Chandar, Y. Bram, B. R. tenOever, O. Elemento, L. B. Ivashkiv, R. E. Schwartz, F. J. Barrat, Sensing of SARS-CoV-2 by pDCs and their subsequent production of IFN-I contribute to macrophage-induced cytokine storm during COVID-19. *Sci. Immunol.* **7**, eadd4906 (2022).
70. J. D. Domizio, M. F. Gulen, F. Saidoune, V. V. Thacker, A. Yatim, K. Sharma, T. Nass, E. Guenova, M. Schaller, C. Conrad, C. Goepfert, L. de Leval, C. von Garnier, S. Berezowska, A. Dubois, M. Gilliet, A. Ablasser, The cGAS–STING pathway drives type I IFN immunopathology in COVID-19. *Nature* **603**, 145–151 (2022).
71. M. Kuka, M. De Giovanni, M. Iannacone, The role of type I interferons in CD4$^+$ T cell differentiation. *Immunol. Lett.* **215**, 19–23 (2019).
72. M. E. Raeber, Y. Zurbuchen, D. Impellizzieri, O. Boyman, The role of cytokines in T-cell memory in health and disease. *Immunol. Rev.* **283**, 176–193 (2018).
73. M. Bhattacharyya, P. Madden, N. Henning, S. Gregory, M. Aid, A. J. Martinot, D. H. Barouch, P. Penaloza-MacMaster, Regulation of CD4 T cells and their effects on immunopathological inflammation following viral infection. *Immunology* **152**, 328–343 (2017).
74. R. S. Akondy, M. Fitch, S. Edupuganti, S. Yang, H. T. Kissick, K. W. Li, B. A. Youngblood, H. A. Abdelsamed, D. J. McGuire, K. W. Cohen, G. Alexe, S. Nagar, M. M. McCausland, S. Gupta, P. Tata, W. N. Haining, M. J. McElrath, D. Zhang, B. Hu, W. J. Greenleaf, J. J. Goronzy, M. J. Mulligan, M. Hellerstein, R. Ahmed, Origin and differentiation of human memory CD8 T cells after vaccination. *Nature* **552**, 362–367 (2017).
75. K. Tucker, J. Branson, M. Dilleen, S. Hollis, P. Loughlin, M. J. Nixon, Z. Williams, Protecting patient privacy when sharing patient-level data from clinical trials. *BMC Med. Res. Methodol.* **16** (Suppl. 1), 77 (2016).
76. T. B. Buus, A. Herrera, E. Ivanova, E. Mimitou, A. Cheng, R. S. Herati, T. Papagiannakopoulos, P. Smibert, N. Odum, S. B. Koralov, Improving oligo-conjugated antibody signal in multimodal single-cell analysis. *eLife* **10**, e61973 (2021).
77. M. Stoeckius, C. Hafemeister, W. Stephenson, B. Houck-Loomis, P. K. Chattopadhyay, H. Swerdlow, R. Satija, P. Smibert, Simultaneous epitope and transcriptome measurement in single cells. *Nat. Methods* **14**, 865–868 (2017).
78. M. Stoeckius, S. Zheng, B. Houck-Loomis, S. Hao, B. Z. Yeung, W. M. Mauck III, P. Smibert, R. Satija, Cell Hashing with barcoded antibodies enables multiplexing and doublet detection for single cell genomics. *Genome Biol.* **19**, 224 (2018).
79. P.-L. Germain, A. Lun, C. Garcia Meixide, W. Macnair, M. D. Robinson, Doublet identification in single-cell sequencing data using *scDblFinder*. *F1000Res.* **10**, 979 (2021).
80. N. Borcherding, N. L. Bormann, G. Kraus, scRepertoire: An R-based toolkit for single-cell immune receptor analysis. *F1000Res.* **9**, 47 (2020).
81. M. Roederer, J. L. Nozzi, M. C. Nason, SPICE: Exploration and analysis of post-cytometric complex multivariate datasets. *Cytometry A* **79A**, 167–174 (2011).
82. C. M. Mousset, W. Hobo, R. Woestenenk, F. Preijers, H. Dolstra, A. B. van der Waart, Comprehensive phenotyping of T cells using flow cytometry. *Cytometry A* **95**, 647–654 (2019).
83. R. V. Luckheeram, R. Zhou, A. D. Verma, B. Xia, CD4$^+$T cells: Differentiation and functions. *Clin. Dev. Immunol.* **2012**, 925135 (2012).
84. D. S. M. Chatzileontiadou, H. Sloane, A. T. Nguyen, S. Gras, E. J. Grant, The many faces of CD4$^+$ T cells: Immunological and structural characteristics. *Int. J. Mol. Sci.* **22**, 73 (2021).
85. Y. Zhou, B. Zhou, L. Pache, M. Chang, A. H. Khodabakhshi, O. Tanaseichuk, C. Benner, S. K. Chanda, Metascape provides a biologist-oriented resource for the analysis of systems-level datasets. *Nat. Commun.* **10**, 1523 (2019).
86. M. I. Love, W. Huber, S. Anders, Moderated estimation of fold change and dispersion for RNA-seq data with DESeq2. *Genome Biol.* **15**, 550 (2014).
87. A. Liberzon, C. Birger, H. Thorvaldsdóttir, M. Ghandi, J. P. Mesirov, P. Tamayo, The Molecular Signatures Database (MSigDB) hallmark gene set collection. *Cell Syst.* **1**, 417–425 (2015).
88. T. Stuart, A. Srivastava, S. Madad, C. A. Lareau, R. Satija, Single-cell chromatin state analysis with Signac. *Nat. Methods* **18**, 1333–1341 (2021).
89. Y. Zhang, T. Liu, C. A. Meyer, J. Eeckhoute, D. S. Johnson, B. E. Bernstein, C. Nusbaum, R. M. Myers, M. Brown, W. Li, X. S. Liu, Model-based analysis of ChIP-Seq (MACS). *Genome Biol.* **9**, R137 (2008).
90. J. A. Castro-Mondragon, R. Riudavets-Puig, I. Rauluseviciute, R. B. Lemma, L. Turchi, R. Blanc-Mathieu, J. Lucas, P. Boddie, A. Khan, N. Manosalva Pérez, O. Fornes, T. Y. Leung, A. Aguirre, F. Hammal, D. Schmelter, D. Baranasic, B. Ballester, A. Sandelin, B. Lenhard, K. Vandepoele, W. W. Wasserman, F. Parcy, A. Mathelier, JASPAR 2022: The 9th release of the open-access database of transcription factor binding profiles. *Nucleic Acids Res.* **50**, D165–D173 (2022).
91. S. L. Gray-Gaillard, CD4T_DifferentialPriming_V1.0.0. Zenodo (2024); https://doi.org/10.5281/zenodo.10814886.

Acknowledgments: We thank all members of NYU Vaccine Center processing and clinical staff, including M. Tuen, J. Wilson, A. Holder, S. Goins, M. Tasissa, S. W. Hyman, and F. Antara. We would like to thank the NYU Genome Technology Core for services, with help from P. Zappile and E. Guzman in particular. Last, we would like to thank all the participants who have contributed to our studies. **Funding:** This work was supported by NIH grants AI082630 (R.S.H.), AI141759 (M.B.O.), AI148574 (M.J.M.), 75N93021C00014 (M.J.M.), AI110830 (S.B.K.), AI137752 (S.B.K.), and HL125816 (S.B.K.); LEO Foundation Grant LF-OC-20-000351 (S.B.K.); Judith and Stewart Colton Center for Autoimmunity Pilot grant (S.B.K.); NCATS/NIH Centers for Translational Science Awards UL1 TR001445; and NYU Langone Health's Laura and Isaac Perlmutter Cancer Center Support grant P30CA016087. **Author contributions:** Conceptualization: S.L.G.-G. and R.S.H. Data curation: S.L.G.-G. Formal analysis: S.L.G.-G.

Funding acquisition: M.B.O., M.J.M., and R.S.H. Investigation: S.L.G.-G., S.M.S., H.M.C., C.M., E.G., M.R., and G.C. Methodology: S.L.G.-G., A.R.C., E.N.I., S.B.K., and R.S.H. Project administration: R.S.H. Supervision: R.S.H. Validation: S.L.G.-G. and R.S.H. Visualization: S.L.G.-G. and R.S.H. Writing—original draft: S.L.G.-G. and R.S.H. Writing—review and editing: S.L.G.-G., S.M.S., H.M.C., C.M., T.W., G.C., A.R.C., M.I.S., E.G., M.B.O., E.N.I., S.B.K., M.J.M., and R.S.H. **Competing interests:** M.J.M. has laboratory research and clinical trials contracts with Lilly, Pfizer (exclusive of the current work), and Sanofi for vaccines or MAB versus SARS-CoV-2, contract funding from USG/HHS/BARDA for research specimen characterization and repository, research grant funding from USG/HHS/NIH for SARS-CoV-2 vaccine and MAB clinical trials, and personal fees from Meissa Vaccines Inc. and Pfizer for Scientific Advisory Board service. R.S.H. has received research support from CareDx for SARS-CoV-2 vaccine studies and has performed consulting work for Bristol-Myers-Squibb (exclusive of the current work). All other authors declare that they have no competing interests. **Data and materials availability:** exCITE-seq and TEA-seq data have been deposited at GEO (GSE233046). All original code is available online at Zenodo (*91*). DEGs, input ranked gene lists for GSEA, and DARs from Figs. 3 to 5 are reported in data S1 to S6. Tabulated underlying data from Figs. 1, 5, 6, and 7 and figs. S1, S6, and S7 are archived in data S7. All other data are available in the main text or the Supplementary Materials.

Submitted 25 July 2023
Accepted 30 May 2024
Published 21 June 2024
10.1126/sciimmunol.adj8526